

# Molecular jets from low-mass young protostellar objects

Chin-Fei Lee

Received: date / Accepted: date

**Abstract** Molecular jets are seen coming from the youngest protostars in the early phase of low-mass star formation. They are detected in CO, SiO, and SO at (sub)millimeter wavelengths down to the innermost regions, where their associated protostars and accretion disks are deeply embedded and where they are launched and collimated. They are not only the fossil records of accretion history of the protostars but also are expected to play an important role in facilitating the accretion process. Studying their physical properties (e.g., mass-loss rate, velocity, rotation, radius, wiggle, molecular content, shock formation, periodical variation, magnetic field, etc) allows us to probe not only the jet launching and collimation, but also the disk accretion and evolution, and potentially binary formation and planetary formation in the disks. Here I review recent exciting results obtained with high-spatial and high-velocity resolution observations of molecular jets in comparison to those obtained in the optical jets in the later phase of star formation. Future observations of molecular jets with a large sample at high spatial and velocity resolution with ALMA are expected to lead to a breakthrough in our understanding of jets from young stars.

**Keywords** Stars: formation · Stars: protostars · ISM: jets and outflows · ISM: Herbig-Haro objects · ISM: magnetic fields · Accretion, accretion disks

## Contents

1	Introduction . . . . .	2
2	Observed properties of molecular jets . . . . .	4
3	Jet rotation . . . . .	7
4	Jet radius near the central source: collimation . . . . .	11
5	Are the jets hollow? . . . . .	13

Academia Sinica Institute of Astronomy and Astrophysics, P.O. Box 23-141, Taipei 106, Taiwan  
E-mail: cflee@asiaa.sinica.edu.tw · Graduate Institute of Astronomy and Astrophysics,  
National Taiwan University, No. 1, Sec. 4, Roosevelt Road, Taipei 10617, Taiwan

6	Shock formation and sideways ejection . . . . .	14
7	Periodical variations and their possible origins . . . . .	16
8	Wiggles and binaries? . . . . .	20
9	Magnetic fields in the jets . . . . .	23
10	Origin of molecular gas in the jets . . . . .	25
11	Disk winds around the jets? . . . . .	26
12	Summaries and conclusions . . . . .	28

## 1 Introduction

Protostellar jets are spectacular signposts of star formation. They are highly collimated structures consisting of a chain of knots and bow shocks, emanating from young protostellar objects, propagating away at highly supersonic speeds. Since they are believed to be launched from accretion disks around protostars, they are not only the fossil records of accretion history of the protostars but also are expected to play an important role in facilitating the accretion process. Studying their dynamics and evolution also allows us to probe disk evolution and potentially planetary formation in the disks.

In low-mass star formation, the protostellar phase with active accretion can be divided into the Class 0 and Class I phases (McKee & Ostriker 2007; Evans et al. 2009; Kennicutt & Evans 2012). The Class 0 phase starts when a protostar is first formed at the center with a mass of  $\sim 10^{-3} M_{\odot}$  and a radius of  $\sim 2 R_{\odot}$  (Larson 1969; Masunaga & Imutsuka 2000). In this phase, the protostar is deeply embedded in a large cold dust envelope and actively accreting material from it. This phase will end in  $\sim 10^5$  yrs when the cold envelope decreases to  $\sim 10\%$  of its original amount (Evans et al. 2009). This phase is then followed by the Class I phase, which will end in  $\sim 5 \times 10^5$  yrs when most of the envelope material has been consumed and the accretion almost comes to an end (Evans et al. 2009). Then the protostar enters the Class II phase or T-Tauri phase, and becomes a pre-main-sequence star visible in the optical. Note that some protostars could already become pre-main-sequence stars earlier during the Class I phase.

Jets are commonly seen in the Class 0 to the early Class II phase when the accretion process is active. Their velocities scale with protostellar mass and thus increase with the evolutionary phase, increasing from  $\sim 100 \text{ km s}^{-1}$  in the early phase to a few  $100 \text{ km s}^{-1}$  in the late phase (Hartigan et al. 2005; Anglada et al. 2007; Hartigan et al. 2011). Therefore, they can propagate for a long distance into the ISM, producing spectacular parsec-scale Herbig-Haro objects (Reipurth & Bally 2001) even in the Class 0 phase (Reipurth et al. 2019, see also Fig. 1 for the Class 0 jet HH 212). When these jets propagate into the ISM, they push and sweep up the surrounding material, forming molecular outflows around the jet axis (Lee et al. 2000; Arce et al. 2007), perturbing the ISM and thus potentially reducing the star-formation efficiency (Bally 2016). Interestingly, jets are also detected around brown dwarfs (e.g., Whelan et al. 2005; Riaz et al. 2017), intermediate-mass protostars (e.g., Zapata et al. 2010; Reiter et al. 2017; Takahashi et al. 2019), and high-mass protostars (Reipurth

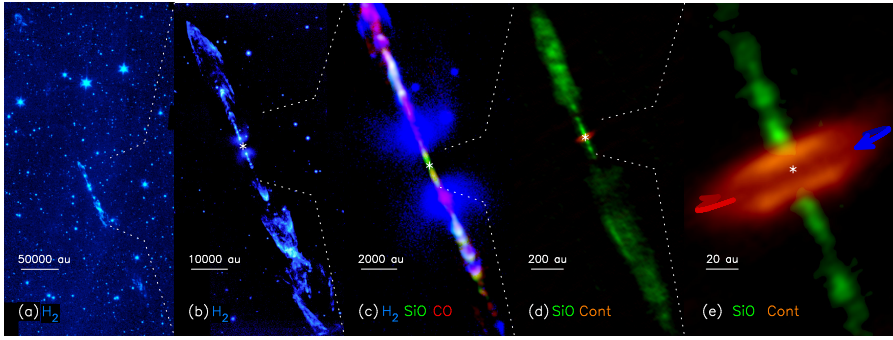


**Fig. 1** HH 212: (a)  $\text{H}_2$  map of the jet in parsec scale adopted from Reipurth et al. (2019). (b)  $\text{H}_2$  map of the inner jet adopted from McCaughrean et al. (2002). (c) A composite image of the jet within  $\sim 10000$  au of the central source, with  $\text{H}_2$  map (blue) from McCaughrean et al. (2002) and SiO (green) and CO (red) maps from Lee et al. (2015). (d) The jet in SiO (green) within  $\sim 1000$  au of the central source and the accretion disk in dust continuum at  $850 \mu\text{m}$  (orange), adopted from (Lee et al. 2017c). (e) shows the SiO jet (green) within  $\sim 100$  au of the central source with the dusty accretion disk (orange), adopted from (Lee et al. 2017c). The blue and red arrows show the disk rotation.

& Bally 2001; Zapata et al. 2006; Carrasco-González et al. 2010; Ellerbroek et al. 2013; Caratti o Garatti et al. 2015), suggesting that the low-mass star formation scenario may apply to these objects.

Current observations also show an evolution in the gas content of the jets. In the Class 0 phase, the jets are mainly detected in molecular gas, e.g., CO, SiO, and SO at (sub)millimeter wavelengths and  $\text{H}_2$  in infrared (Arce et al. 2007; Frank et al. 2014). In the Class I and Class II phases, they are mainly detected in atomic and ionized gas, e.g., O,  $\text{H}\alpha$ , and S II (Reipurth & Bally 2001; Bally 2016), appearing as Herbig-Haro flows at optical and infrared wavelengths. At the base near the launching points, the jets are ionized and thus radiate free-free emission at centimeter wavelengths (Anglada et al. 2018). Therefore, different telescopes are used to study different regions of the jets in different evolutionary phases.

Recent comprehensive reviews of the jets have been presented by Frank et al. (2014) and Bally (2016), and a further review on radio jets by Anglada et al. (2018). Here I will focus on molecular jets seen in the early phase of low-mass star formation, probing the initial phase of the jet formation and accretion process in the first  $10^5$  yrs in the Class 0 phase. Without suffering from dust extinction effects, molecular lines at (sub)millimeter wavelengths allow us to probe the jets close to the innermost regions, where the sources are deeply embedded and where the jets are launched and collimated (see Fig. 1). The jets are believed to be launched from accretion disks around protostars through magneto-centrifugal forces (Shu et al. 2000; Königl & Pudritz 2000), and are thus expected to be magnetized and rotating. In this case, the jets can also solve the angular momentum problem in the innermost edges of the disks by carrying away angular momentum from there to allow disk material to fall onto the central protostars. I will review current exciting and revolutionary

**Table 1** Molecular jets from low-mass Class 0 protostars detected in both SiO and CO

Source	$D$ (pc)	$L_{\text{bol}}$ ( $L_{\odot}$ )	$M_*$ ( $M_{\odot}$ )	$r_d$ (au)	$v_j$ (km/s)	$\dot{M}_j$ ( $M_{\odot} \text{ yr}^{-1}$ )	$L_j$ $L_{\odot}$	$\dot{M}_{\text{acc}}$ ( $M_{\odot} \text{ yr}^{-1}$ )	Refs.
IRAS 04166+2706	140	0.4		?	61	$0.7 \times 10^{-6}$	0.21		1
B335	100	0.7	0.05	$< 5$	160	$0.1 \times 10^{-6}$	0.21	$1.2 \times 10^{-6}$	2
NGC1333 IRAS4A2	320	3.5	0.11	$< 65$	100				3
L1157	250	3.6	0.04	$< 50$	112	$0.8 \times 10^{-6}$	0.82	$7.1 \times 10^{-6}$	4
HH 211	320	4.7	0.08	16	100	$1.1 \times 10^{-6}$	1.1	$4.7 \times 10^{-6}$	5
L1448 C	320	8.4	0.08	50?	160	$2.4 \times 10^{-6}$	5.0	$11 \times 10^{-6}$	6
HH 212	400	9.0	0.25	44	135	$1.3 \times 10^{-6}$	1.9	$2.8 \times 10^{-6}$	7

Here  $D$  is distance,  $L_{\text{bol}}$  is bolometric luminosity,  $M_*$  is mass of central protostar,  $r_d$  is disk radius,  $v_j$  is jet velocity,  $\dot{M}_j$  is mass-loss rate in the jet,  $L_j$  is mechanical luminosity of the jet, and  $\dot{M}_{\text{acc}}$  is accretion rate. References: (1) [Santiago-García et al. \(2009\)](#), [Tafalla et al. \(2017\)](#) (2) [Yen et al. \(2010\)](#), [Green et al. \(2013\)](#), [Bjerkeli et al. \(2019\)](#) (3) [Choi et al. \(2006, 2010, 2011\)](#) (4) [Green et al. \(2013\)](#), [Kwon et al. \(2015\)](#), [Podio et al. \(2016\)](#), [Maury et al. \(2019\)](#) (5) [Froebrich \(2005\)](#), [Lee et al. \(2018b\)](#), [Jhan & Lee \(2016\)](#) (6) [Hirano et al. \(2010\)](#), [Green et al. \(2013\)](#), [Maury et al. \(2019\)](#) (7) [Zinnecker et al. \(1998\)](#), [Lee et al. \(2017a,c\)](#)

results on molecular jets, especially those obtained with unprecedented angular resolution, velocity resolution, and sensitivity using ALMA. Together with previous detailed studies of jets in their later phase, we can set strong constraints on jet launching and collimation. With a detailed study of jet physical properties (e.g., mass-loss rate, velocity, rotation, radius, wiggle, molecular content, shock formation, periodical variation, magnetic field, etc), we can also probe accretion process, binary formation, disk instability and evolution, and potentially planetary formation in the disks.

## 2 Observed properties of molecular jets

Protostellar jets in the Class 0 phase are mainly molecular. They can be traced by high-velocity CO emission ([Gueth & Guilloteau 1999](#); [Lee et al. 2007](#); [Santiago-García et al. 2009](#); [Hirano et al. 2010](#); [Plunkett et al. 2015](#)), which allows us to derive the density and thus the mass-loss rate in the jets. Their knots and bow shocks can be traced by shock tracers, e.g.,  $\text{H}_2$  ([McCaughrean et al. 1994](#); [Zinnecker et al. 1998](#)), SiO ([Gueth et al. 1998](#); [Hirano et al. 2006](#); [Palau et al. 2006](#); [Codella et al. 2007](#); [Lee et al. 2007](#); [Codella et al. 2014](#); [Podio et al. 2016](#); [Bjerkeli et al. 2019](#)), and SO ([Lee et al. 2007, 2010](#); [Codella et al. 2014](#)). More importantly, SiO is a dense shock tracer, tracing uniquely the jets within  $\sim 10^4$  au of the central sources down to the bases where the density is high, allowing us to probe the jet launching and collimation regions.

Table 1 lists the properties of a few well-studied molecular jets from low-mass Class 0 protostars detected in both SiO and CO at (sub)millimeter wavelengths. Note that although the jets listed here are bipolar, there are also monopolar jets, e.g., in NGC1333-IRAS2A ([Codella et al. 2014](#)). This table also lists the mechanical luminosity of the jets calculated from the following equation

$$L_j = \frac{1}{2} \dot{M}_j v_j^2 \approx 0.82 \frac{\dot{M}_j}{10^{-6} M_\odot \text{ yr}^{-1}} \left( \frac{v_j}{100 \text{ km s}^{-1}} \right)^2 L_\odot \quad (1)$$

and the accretion rate onto the protostars estimated from the following equation

$$\dot{M}_{\text{acc}} \sim \frac{(L_{\text{bol}} + L_j) R_*}{GM_*} \approx 6.44 \times 10^{-8} \frac{L_{\text{bol}} + L_j}{L_\odot} \frac{M_\odot}{M_*} M_\odot \text{ yr}^{-1} \quad (2)$$

assuming that both the bolometric luminosity and the jet's mechanical luminosity come from accretion. Here we assume the radius of the central protostars is  $R_* \sim 2 R_\odot$  (Stahler 1988). Rotating disks have been detected or suggested in most of these sources, as required in current magneto-centrifugal models of jet launching (Shu et al. 2000; Königl & Pudritz 2000).

Although the sample is small and the measurements have significant uncertainties, we still can see some trends in comparison to the jets in the later phase of star formation. The mass of the protostars is  $0.05\text{--}0.25 M_\odot$ , smaller than that in the Class I and II phases (see, e.g., Simon et al. 2000; Yen et al. 2017). Thus, the mass in most of the protostars here might be too small to have deuterium burning (Stahler 1988). The jet velocity is  $61\text{--}160 \text{ km s}^{-1}$ , much smaller than that of the Class I and II jets. The mass-loss rate is  $(0.7\text{--}2.4) \times 10^{-6} M_\odot \text{ yr}^{-1}$  (except for B335 with a much smaller value), and is much larger than those in the Class I and II phases. The jets have a mechanical luminosity about 20–50% of the bolometric luminosity. The accretion rate is a few times the mass-loss rate. The disks and candidate disks mostly have a radius  $r_d < 50 \text{ au}$ , smaller than those in the Class I phase, as discussed in Maury et al. (2019).

The ratio of the mass-loss rate to the accretion rate has been used to probe the mass-ejection efficiency that is then compared to the current jet-launching models. Figure 2 shows the mass-loss rate versus the accretion rate for the Class 0 jets here (as marked with blue stars) in comparison to those found in different classes of young stellar objects (YSOs) associated with jets and outflows presented in Ellerbroek et al. (2013). As can be seen, our data points follow roughly the trend found before, which shows the mass-loss rate and accretion rate decreasing from the Class 0 to Class II (T-Tauri) phase from  $10^{-6}$  to  $10^{-10} M_\odot \text{ yr}^{-1}$  and from  $10^{-5}$  to  $10^{-9} M_\odot \text{ yr}^{-1}$ , respectively. Our data points here are in the higher end with higher mass-loss rate and accretion rate, because the jet sources here are younger. A linear fit to our data points results in a ratio  $\frac{\dot{M}_j}{\dot{M}_{\text{acc}}} \sim 0.19$ , higher than  $\sim 0.12$  obtained by fitting to all the Class 0/I data points. However, since the data distribution is rather scattered and our sample is small, further work with more accurate measurements are needed to check this. Nonetheless, both ratios are consistent with magneto-centrifugal jet-launching models. Note that in current jet-launching models, there will be wide-angle wind components around the jets, thus the mass-loss

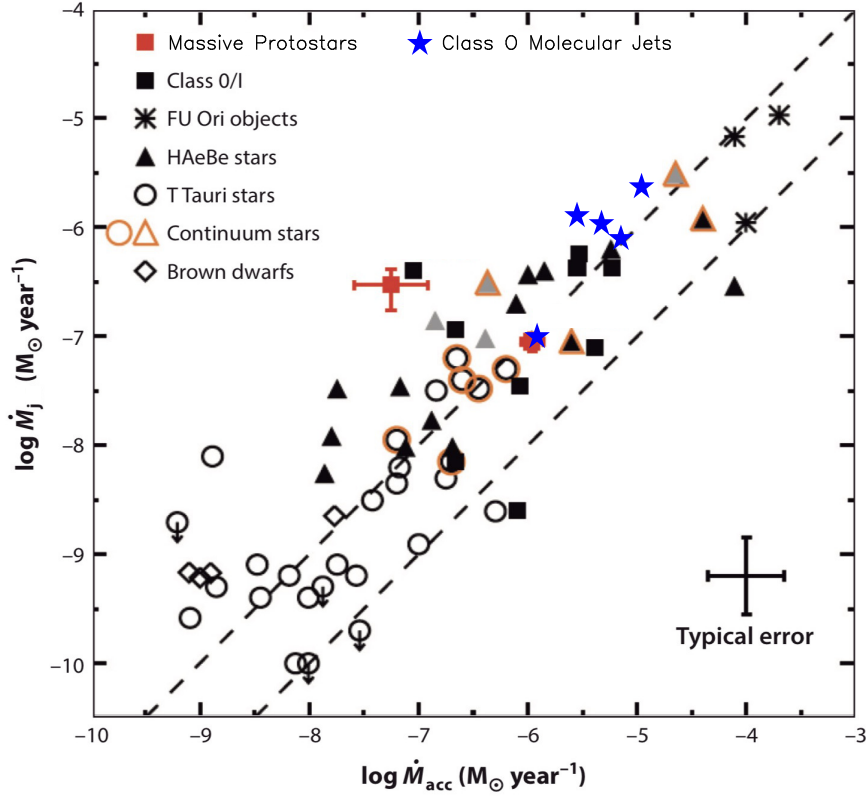


**Fig. 2** Observed mass-loss rate in the jets  $\dot{M}_j$  versus accretion rate  $\dot{M}_{\text{acc}}$  of our jet sources (blue stars) compared with those in different classes of YSOs associated with jets and outflows presented in [Ellerbroek et al. \(2013\)](#). The dashed lines indicate  $\frac{\dot{M}_j}{\dot{M}_{\text{acc}}} = 0.01$  and  $0.1$ .

rate estimated here could be a lower limit of the true value, and so could be the ratio.

With the ratio, we can estimate the magnetic lever arm parameter ([Shu et al. 2000](#); [Pudritz et al. 2007](#)), which is defined as

$$\lambda \equiv \left( \frac{r_A}{r_0} \right)^2 \approx \frac{\dot{M}_{\text{acc}}}{\dot{M}_j} \quad (3)$$

where  $r_0$  is the launching radius of the jets in the disks and  $r_A$  is the Alfvén radius along the streamline launched from  $r_0$ . This parameter determines the extracted angular momentum and poloidal acceleration, assuming a conservation of angular momentum and energy along the streamline. For example, the poloidal acceleration determines the terminal velocity the jet can achieve. Let  $v_{\text{kep}}$  be the Keplerian velocity at the launching point, then  $v_j \sim \sqrt{2\lambda - 3} v_{\text{kep}}$ , according to the current magneto-centrifugal jet-launching models ([Shu et al.](#)

2000; Pudritz et al. 2007). Thus, with a given protostellar mass and jet velocity, we can derive the launching radius with

$$r_0 \sim (2\lambda - 3) \frac{GM_*}{v_j^2} \quad (4)$$

Based on Table 1 using the 6 sources with both mass and jet velocity measured, the jet sources have a mean mass of  $M_* \sim 0.10 M_\odot$  and the jets have a mean velocity of  $v_j \sim 130 \text{ km s}^{-1}$ . Then with a mean  $\lambda \sim 1/0.19 \sim 5$  for our jet sources, the mean jet launching radius is  $\sim 0.04 \text{ au}$ , which is  $\sim 4 R_*$ . Further observations of a larger sample with better measurements of all related quantities are needed to refine this.

### 3 Jet rotation

In current jet-launching models, the jets are launched by magneto-centrifugal force from the innermost parts of the disks, and are thus expected to be rotating and magnetized. In this way, angular momentum can be carried away by the jets from the innermost parts of the disks, allowing material there to actually fall onto the central protostars. Therefore, measuring jet rotation is an important task to confirm these models and the role of the jets in removing the angular momentum from the disks. The measured amount of angular momentum in the jets can also help us differentiate between the two competing models of jet launching, namely, the X-wind model (Shu et al. 2000) and the disk-wind model (Königl & Pudritz 2000), without spatially resolving the launching zones on the  $\sim 0.05 \text{ au}$  scale. These two models predict different amounts of angular momentum to be carried away by the jets. In particular, the jets in the X-wind model are launched from the innermost edge of the disks and thus carry only a small amount of specific angular momentum of  $\lesssim 10 \text{ au km s}^{-1}$  (Shu et al. 2000), while the jets in the disk-wind model are launched from a range of radii from the innermost edge out to  $\sim 1 \text{ au}$ , and thus can carry a larger amount of specific angular momentum up to a few 100  $\text{au km s}^{-1}$  (Pudritz et al. 2007).

Previously, jet rotation was tentatively detected in T-Tauri jets in optical [OI], [NII], and [SII] lines using the STIS instrument aboard the *Hubble Space Telescope*, with a velocity sampling of  $\sim 25 \text{ km s}^{-1} \text{ pixel}^{-1}$  and a spatial sampling of  $\sim 7 \text{ au}$  (or  $0''.05$  in Taurus)  $\text{pixel}^{-1}$  (Bacciotti et al. 2002; Coffey et al. 2007). The jets were found to have a specific angular momentum up to a few 100  $\text{au km s}^{-1}$ , suggesting a launching radius of 0.2 to 1  $\text{au}$  (Coffey et al. 2007). Similar measurements were also made towards a few Class 0 jets, e.g., HH 212 (with a spatial resolution of  $\sim 140 \text{ au}$  and a velocity resolution of  $\sim 1 \text{ km s}^{-1}$ , Lee et al. 2008), HH 211 (with a spatial resolution of  $\sim 77 \text{ au}$  and a velocity resolution of  $\sim 0.35 \text{ km s}^{-1}$ , Lee et al. 2009), and NGC 1333 IRAS 4A (with a spatial resolution of  $\sim 480 \text{ au}$  and a velocity resolution of  $\sim 0.67 \text{ km s}^{-1}$ , Choi et al. 2011) in SiO at radio wavelengths, finding a launching radius of 0.03 to 2  $\text{au}$ . Tentative jet rotation was also reported in the Class I jet HH 26

(with a spatial sampling of  $\sim 60$  au and a velocity resolution of  $\sim 34$  km s $^{-1}$ , Chrysostomou et al. 2008) in H $_2$ , suggesting a launching radius of 2 to 4 au. Tentative jet rotation was also reported in SO in the intermediate-mass source Ori-S6 (Zapata et al. 2010), suggesting a launching radius of  $\sim 50$  au. However, all of these measurements are based on shock emission (e.g., SiO, SO, H $_2$ , and [OI]) and thus could be uncertain if the shock structures and kinematics of the jets are not spatially resolved, for example, the rotation in T-Tauri jets was later found to be false (Coffey et al. 2012). In addition, asymmetric shock structure and jet precession can also produce a velocity gradient mimicking a jet rotation.

Since the jets are highly collimated and narrow, a spatial resolution of better than 10 au is needed to spatially resolve them. In addition, since the rotation speed is small in the jets, a velocity resolution of  $\sim 1$  km/s is also needed to detect it. More importantly, we need to zoom in to the innermost parts of the jets, where the (internal) shocks have not yet developed significantly, where the jets are not yet interacting significantly with the surrounding and cavity material, and where the jet precession effect is not significant, so that the rotation signature can be preserved and the velocity gradient across the jet axis can be attributed to jet rotation. Moreover, since the jet radius decreases towards the central source as discussed later, we also need to avoid zooming in too close to the central source where the jets become unresolvable with current instruments.

Thanks to the powerful Atacama Large Millimeter/submillimeter Array (ALMA) with an unprecedented combination of high spatial resolution of  $\sim 8$  au and high velocity resolution of  $\sim 1$  km s $^{-1}$ , Lee et al. (2017c) reported a more reliable detection of jet rotation in the Class 0 jet HH 212 in SiO. This jet is almost in the plane of the sky, allowing us to measure the jet rotation without being affected by projection effects. In this jet, six knots (N1, N2, N3 and S1, S2, S3) were detected in SiO within 100 au of the central source, with three on each side, as shown in Figure 3a. As shown in Fig. 3b, the blueshifted emission and redshifted emission are on the opposite sides of the jet axis, showing a consistent velocity gradient with the same velocity sense as the disk rotation, indicating that the velocity gradient is due to jet rotation. Note that although the inner knots are less resolved, they still show a hint of velocity gradient with the same velocity sense as the outer knots. This measurement strongly supports the role of the jet in carrying away the angular momentum from the disk. Based on the position-velocity diagrams across the knots in the jet (Fig. 4), the specific angular momentum in the knots is estimated to be  $\sim 10$  au km s $^{-1}$ , but could be smaller because the knots are not well resolved spatially.

In the framework of magneto-centrifugal jet-launching models, the jet is the central core of a magnetized wind. The launching radius at the foot point of the jet in the accretion disk can be derived from the observed specific angular momentum and the observed velocity of the jet at a large distance from the central source, assuming a conservation of energy and angular momentum along the field line. In addition, the wind can be assumed to have enough



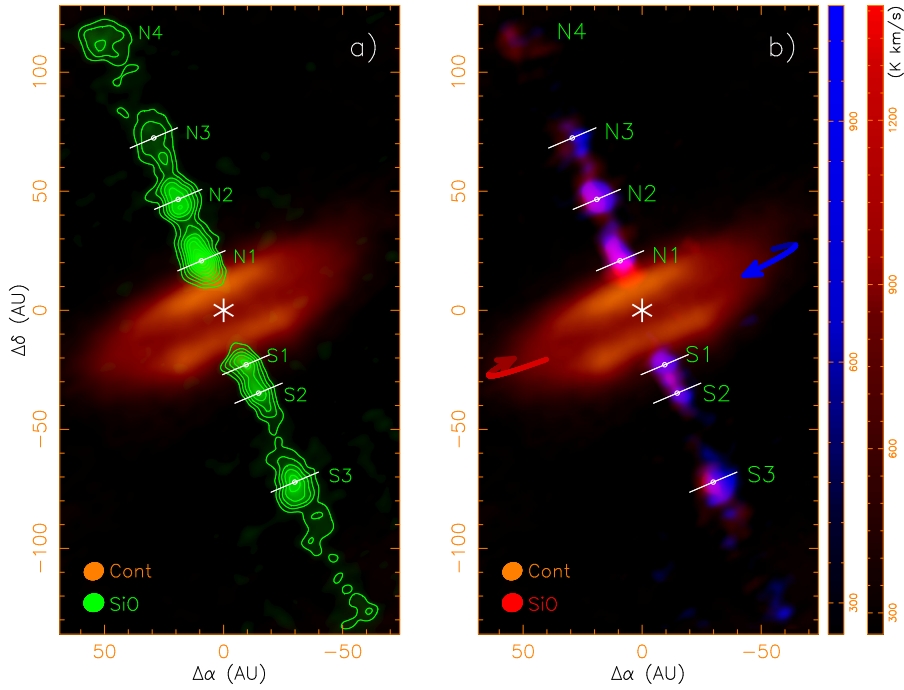


**Fig. 3** ALMA results of the SiO jet in HH 212 within 100 au of the central source, adopted from Lee et al. (2017c). The orange image shows the dusty disk observed at 850  $\mu\text{m}$  (Lee et al. 2017a). In (a), the green image shows the SiO jet. In (b), blueshifted emission and redshifted emission are plotted separately to show the jet rotation around the jet axis. The blue and red arrows show the disk rotation.

energy to climb out of the potential well of the central star easily, so that the kinetic energy of the wind is substantially greater than the gravitational binding energy at the launching surface. With these assumptions, Anderson et al. (2003) has derived a useful relation between the angular momentum at large distance and the jet launching radius ( $r_0$ ) at the foot point of the field line in the disk:

$$r_0 \approx 0.7 \text{ au} \left( \frac{l_j}{100 \text{ au km s}^{-1}} \right)^{2/3} \left( \frac{v_j}{100 \text{ km s}^{-1}} \right)^{-4/3} \left( \frac{M_*}{1 M_\odot} \right)^{1/3} \quad (5)$$

where  $l_j$  and  $v_j$  are the specific angular momentum and velocity of the jet at large distance. In the case of HH 212 where  $l_j$  is small, we need to add two correction terms to the above solution as in the following (Lee et al. 2017c)

$$r_0 \approx 0.7 \text{ au} \left( \frac{l_j}{100 \text{ au km s}^{-1}} \right)^{2/3} \left( \frac{v_j}{100 \text{ km s}^{-1}} \right)^{-4/3} \left( \frac{M_*}{1 M_\odot} \right)^{1/3} \left[ 1 - \frac{2}{3}\eta + \frac{1}{9}\eta^2 \right] \quad (6)$$

with

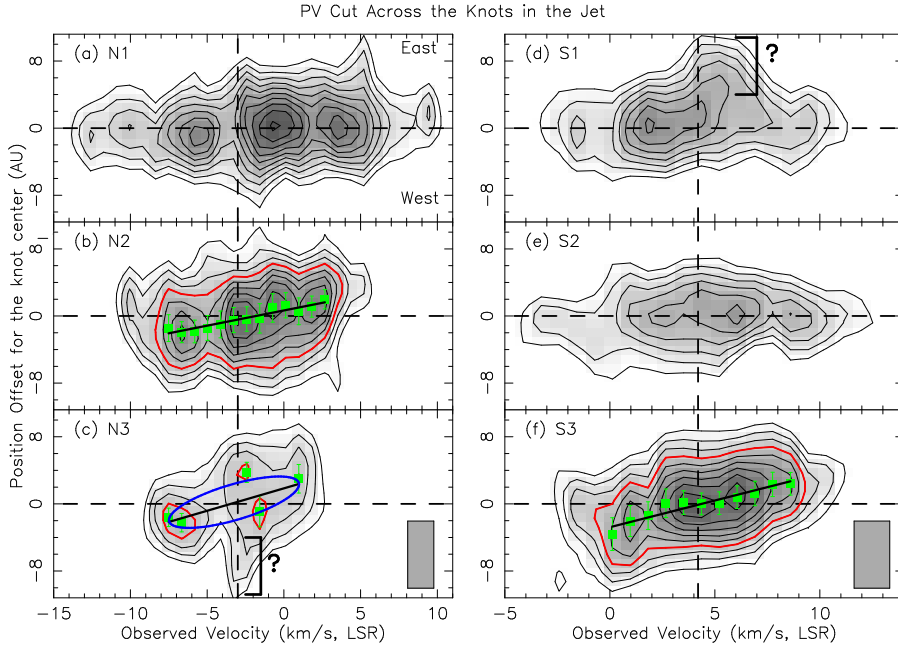


**Fig. 4** Position-velocity (PV) diagrams cut across the knots (N1-N3 and S1-S3) in the HH 212 jet, adopted from Lee et al. (2017c). The horizontal dashed lines indicate the peak (central) position of the knots. The vertical dashed lines indicate roughly the systemic (mean) velocities for the northern and southern jet components. The red contours mark the  $7\sigma$  detections in knots N2, N3 and S3. The solid lines mark the linear velocity structures across the knots due to the jet rotation. In (c), the blue ellipse is a tilted elliptical PV structure expected for a rotating and expanding ring (see text).

$$\eta = \frac{3}{2^{2/3}} \left( \frac{GM_*}{v_j l_j} \right)^{2/3} \approx 0.38 \left( \frac{l_j}{100 \text{ au km s}^{-1}} \right)^{-2/3} \left( \frac{v_j}{100 \text{ km s}^{-1}} \right)^{-2/3} \left( \frac{M_*}{1 M_\odot} \right)^{2/3}. \quad (7)$$

The two correction terms can improve the accuracy of the launching radius estimate in the case where the dimensionless parameter  $\eta$  is not much smaller than unity, particularly when the specific angular momentum  $l_j$  is relatively small, as is true for HH 212. Then with  $l_j \sim 10 \text{ au km s}^{-1}$ ,  $v_j \sim 135 \text{ km s}^{-1}$ , and  $M_* \sim 0.25 M_\odot$  (see Table 1), the launching radius of the HH 212 jet is estimated to be  $\sim 0.04 \text{ au}$ , consistent with current models of jet launching. This results in a magnetic lever arm parameter of  $\lambda \sim 3.2$  (see Eq. 4), indicating that the jet has a specific angular momentum about 3 times that in the disk at the launching radius. Since the mass-loss rate in the jet is estimated to be  $\sim 1.3 \times 10^{-6} M_\odot$  (see Table 1), the angular momentum flux would be  $1.3 \times 10^{-5} M_\odot \text{ au km s}^{-1} \text{ yr}^{-1}$ . Fig. 5 shows a possible scenario of the jet launching in HH 212 from the accretion disk. In the innermost part of the disk, part of the disk material is ejected, forming a bipolar jet carrying the

angular momentum away, allowing the disk material to fall onto the central protostar through a funnel flow (Shu et al. 2000).

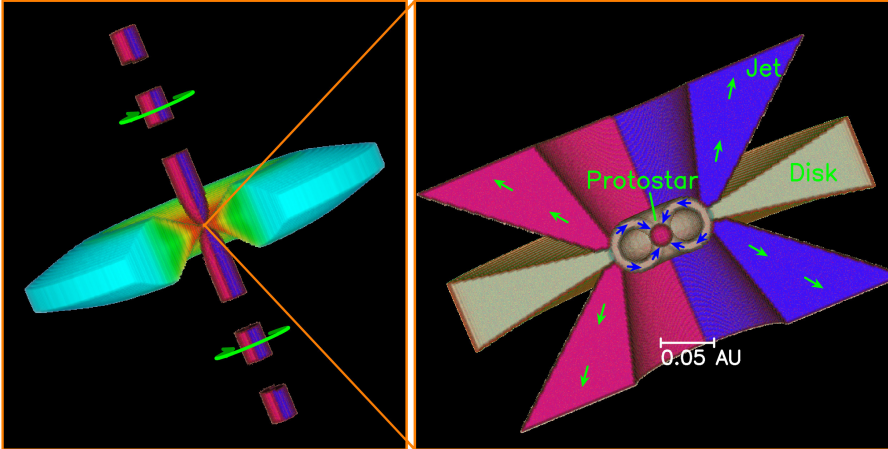


**Fig. 5** Cartoon showing a possible jet launching scenario for HH 212. In the innermost part of the disk, part of the disk material is ejected, forming a bipolar jet carrying the angular momentum away, allowing the disk material to fall onto the central protostar through a funnel flow.

Recent ALMA observations at an unprecedented high resolution of  $\sim 3$  au have detected a small SiO jet in B335 extending out from the central source along the outflow axis (Bjerkeli et al. 2019, see also Fig. 6). This jet is located within  $\sim 4$  au of the central source and has a radius of  $\lesssim 1$  au. No clear rotation is detected in this jet, likely because the jet is not resolved at current resolution. In addition, since the central source seems to have a smaller protostellar mass of only  $\sim 0.05 M_{\odot}$  (Bjerkeli et al. 2019), the jet rotation is expected to be smaller than that seen in HH 212 and is thus more difficult to detect. The SiO line in this jet has a linewidth of  $\sim 13$  km s $^{-1}$  (Bjerkeli et al. 2019). Assuming that this linewidth is mainly due to jet rotation, then the specific angular momentum of the jet is  $\lesssim 6.5$  au km s $^{-1}$ . If this is the case, then the jet launching radius would be  $\lesssim 0.02$  au, assuming a jet velocity of 160 km s $^{-1}$  (see Table 1). Further observations are needed to check this.

#### 4 Jet radius near the central source: collimation

With the unprecedented angular resolutions of ALMA, we can now measure the radius of molecular jets within 100 au of the central sources in order to probe the collimation zones, as done before for T-Tauri jets in the optical. Figure 7 shows the radii of the jets in the two Class 0 sources HH 212 (assumed to be half of the Gaussian widths reported in Lee et al. 2017c) and B335 (measured from the SiO maps shown in Fig. 6 adopted from Bjerkeli et al.

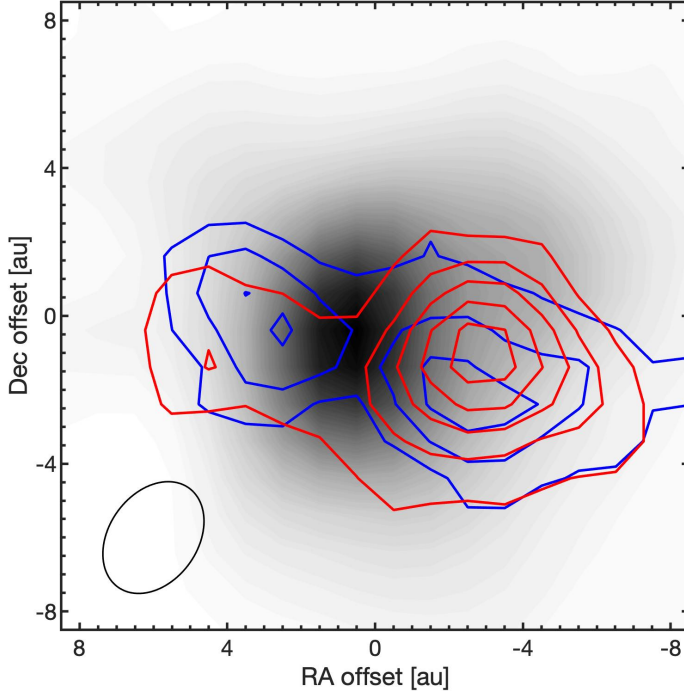


**Fig. 6** SiO maps of the jet in B335 obtained with ALMA at  $\sim 3$  au resolution (Bjerkeli et al. 2019). Blue and red contours show the blueshifted and redshifted emission maps of the jet in SiO J=5-4.

2019) in comparison to those in the two T-Tauri sources, RW Aur (Woitas et al. 2002) and DG Tau (Agra-Amboage et al. 2011), previously measured from the high-velocity emission maps in the optical. As seen from the figure, the Class 0 jets seem to be narrower and have a smaller expansion rate in jet radius with distance than the T-Tauri jets. However, further work with a larger sample is needed to confirm it. Interestingly, for both types of jets, the jet radius could be increasing roughly parabolically with the distance (i.e., with the square of the distance), as guided by the gray shaded area in the figure, and thus roughly consistent with that predicted in current magneto-centrifugal models of jet launching (Shu et al. 2000; Königl & Pudritz 2000). In these models, the jets are collimated internally by their own toroidal magnetic fields and expand roughly parabolically with the distance. If the jet radius indeed expands roughly parabolically with the distance, then the jets must have launched from the innermost parts of the disks within a radius much less than 1 au of the central sources, as guided by the gray shaded area.

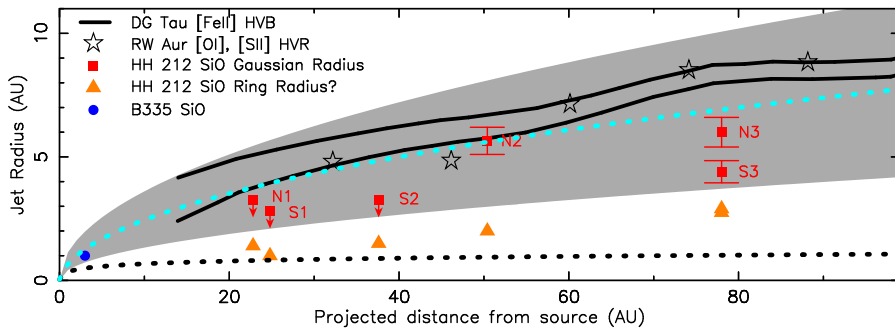


**Fig. 7** Observed jet radius versus the distance from the central source. Here, DG Tau data points are adopted from [Agra-Amboage et al. \(2011\)](#), RW Aur from [Woitas et al. \(2002\)](#), HH 212 from [Lee et al. \(2017c\)](#), and B335 from [Bjerkeli et al. \(2019\)](#). Note that in HH 212, the radius of knot N3 in HH 212 has been revised to be  $\sim 6$  au here after excluding the emission in the west around  $-3 \text{ km s}^{-1}$  (see Fig. 4c, marked with a “?”), which could result from an interaction with the material in the cavity. The gray shaded area is to guide the readers that the jet radius could be increasing roughly parabolically with the distance. The black dotted curve outlines the radius of a hollow cone in an X-wind launched at a radius of 0.04 au. The cyan dotted curve indicates the streamline within which the X-wind contains 30% of the total mass-loss rate. The orange triangles indicate the radius of the SiO knots in HH 212, assuming the SiO emission comes from a ring (see text).

## 5 Are the jets hollow?

In current magneto-centrifugal jet-launching models, there is a narrow hollow cone in the jet center along the jet axis because of an intrinsic expansion of the magneto-centrifugal winds coming from the disks. This hollow cone is also supported by an axially opened stellar magnetic field. However, there will be no hollow cone if the jets turn out to be stellar winds launched by stellar magnetic field. Therefore, it is critical to check for the existence of a hollow cone in the jets in order to determine the jet-launching models.

Here we can compare the observed radius of the HH 212 molecular jet to the predicted radius of the hollow cone in the X-wind model ([Shu et al. 2000](#)). Since the launching radius of the jet is estimated to be  $\sim 0.04$  au, we calculate the predicted radius of the hollow cone for this launching radius, as shown as the black dotted curve in Fig. 7. For comparison, we also plot the streamline (the cyan dotted curve) within which the X-wind contains 30% of the total mass-loss rate. As can be seen, the radius of the knots of HH 212 is larger than that of the hollow cone, indicating that we can not rule out the existence of a hollow cone in this jet. In addition, the radius of the knots is smaller than the cyan streamline, supporting that the jet traces the inner core of the wind.

We can also check the existence of the hollow cone by investigating the kinematics. The outer SiO knots (i.e., N2, S3, and N3) are roughly resolved. The position-velocity (PV) diagrams across them show a roughly linear PV structure (see Fig. 4), suggesting that they could actually be rotating rings, as expected if there is a hollow cone in the jet. For knot N3, the PV diagram even shows a tilted elliptical PV structure (blue ellipse in Fig. 4c), as expected for

a rotating ring with an expansion (Lee et al. 2018a). Although the inner knots (i.e., N1, S1, and S2) are not resolved, knots N1 and S2 also seem to show the similar linear PV structure, suggesting that they could also be rotating rings. As a result, the kinematics across the knots in the HH 212 jet is consistent with a presence of a hollow cone in the jet. If this is the case, the radius of the knot is better assumed to be the radius of the ring rather than the Gaussian radius. Assuming that the SiO emission of each knot comes from a ring, we can estimate the ring radius using the two ends of the linear velocity structures in the PV diagrams. As can be seen, the ring radius of the knots (marked as orange triangles) is slightly larger than that of the hollow cone, supporting that the SiO knots come from the innermost core of the wind and the jet is hollow.

Since knot N3 shows an expansion in the PV diagram, we can also check if its expansion velocity can be consistent with the intrinsic expansion velocity of a magneto-centrifugal wind. A rough fit (blue ellipse in Figure 4c) to the PV structure suggests an expansion velocity of  $\sim 3 \text{ km s}^{-1}$  in this knot. Since the jet has a velocity of  $\sim 135 \text{ km s}^{-1}$ , this expansion velocity would require a streamline with a very small angle of  $\sim 1.3^\circ$  to the jet axis, and thus consistent with a streamline in the innermost core of the wind around the possible hollow cone.

## 6 Shock formation and sideways ejection

Studying the formation of the knots and bow shocks in the molecular jets allows us not only to further constrain the origins of the jets but also to understand the jet chemistry. Since the molecular jets, e.g., HH 211 (Gueth & Guilloteau 1999; Lee et al. 2010), HH 212 (Lee et al. 2008, 2015), and L1448 C (Hirano et al. 2010), appear to be continuous in the inner parts, the jet ejection at the base should be continuous. Some of them show roughly equal spacings in between knots and bow shocks, indicating that the knots and bow shocks are produced by quasi-periodical variations in ejections. Since the knots and bow shocks are well detected in, e.g., SiO and H<sub>2</sub>, they trace strong shocks, as in the optical jets (Ray et al. 2007; Hartigan et al. 2011; Bally 2016). Therefore, they can not merely trace quasi-periodical ejections of enhanced jet densities, which alone would not produce shocks (Frank et al. 2014). There must also be a quasi-periodical variation in ejection velocity, so that a shock can be formed as the fast jet material catches up with the slow jet material. A simple form of velocity variation is a sinusoidal variation, presumably induced by an orbital motion of the perturbations. An eccentric orbit can even cause an enhanced accretion rate and thus mass-ejection rate near periastrons (Reipurth 2000; Benisty et al. 2013).

Many hydrodynamical simulations have been performed to study the formation of knots and bow shocks with a periodical sinusoidal variation of ejection velocity (e.g., Raga et al. 1990; Stone & Norman 1993; Suttner et al. 1997; Lee et al. 2001). In the body of the jet, the fast material catches up with

the slower material, forming an internal shock (which consists of a forward shock, a backward shock, and an internal working surface in between). This internal shock is first seen as a knot. As it propagates down along the jet axis, because of sideways ejection in the shock, it expands laterally and grows to a wider knot and then a bow shock and then an internal shell of post-shock gas closing back to the central source (Lee et al. 2001). Each bow shock will show a spur velocity structure in the PV diagram along the jet axis (Lee et al. 2001; Ostriker et al. 2001), because the gas velocity decreases rapidly away from the bow tip. If the amplitude of the velocity variation is larger, the resulting bow shock is bigger.

A periodical variation in jet velocity has been suggested in the jet in L1448 C (Hirano et al. 2010). In particular, each SiO knot has its higher velocity in the upstream (closer to the jet source) side and lower velocity in the downstream side. The opposite velocity gradient is always seen in the faint emission between the knots. Such a velocity pattern is likely to be formed by a periodical variation in the ejection velocity, as seen in the simulations (Stone & Norman 1993; Suttner et al. 1997). In HH 211 (a jet close to the plane of the sky), the innermost pair of jetlike structures BK1 and RK1, which consists of a chain of smaller subknots, show a velocity range decreasing with distance (Lee et al. 2010), also as expected for the knots being formed by a periodical variation in velocity (Suttner et al. 1997). The two knots further away are believed to be newly formed internal shocks, each showing a pair of backward and forward shocks expanding longitudinally with time (Jhan & Lee 2016). In these jets, a velocity variation of 20–30 km s<sup>-1</sup> has been suggested to produce the knots that have a spacing corresponding to a period of a few ten yrs (Hirano et al. 2010; Jhan & Lee 2016).

A clear example showing the sideways ejection of the internal shocks is the molecular jet in IRAS 04166+2706. It consists of at least 7 pairs of knots seen in SiO and CO, with the width increasing with distance from the central source (Santiago-García et al. 2009, see also Fig. 8 left). The velocity field along the jet axis shows a sawtooth pattern for each knot. This pattern, together with a systematic widening of the knots with distance to the central source, is consistent with them tracing the laterally-expanding internal shocks viewed at a high inclination angle to the plane of the sky (Stone & Norman 1993; Suttner et al. 1997). At a large distance from the central source, the knots, B6 and R6, have grown to possess bow-like structures. A detailed kinematic study of this pair of knots with ALMA confirmed that they are internal bow shocks where material is being ejected laterally away from the jet axis (Tafalla et al. 2017), as shown in Fig. 8.

Sideways ejection is also detected in other jets. In HH 212, the sideways ejection is clearly seen in the two spatially resolved internal bow-like knots SK4 and SK5 in CO and SiO (Lee et al. 2015). Since the HH 212 jet is almost in the plane of the sky, the knots are associated with arclike velocity patterns (Stone & Norman 1993), instead of a sawtooth velocity pattern seen in a highly inclined jet. Nested internal shells are also seen in CO, with each extending from a H<sub>2</sub> bow shock back to the central source (Lee et al. 2015), as seen

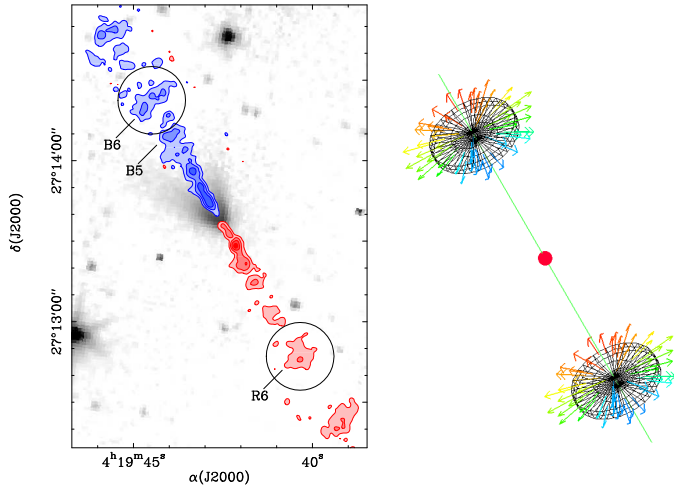


**Fig. 8** Molecular jet in IRAS 04166+2706: (Left) A chain of knots are detected in CO along the jet axis (Santiago-García et al. 2009). (Right) A schematic diagram showing the sideways ejection in knots B6 and R6, as concluded from a detailed ALMA kinematic study (Tafalla et al. 2017).

in the simulations. Sideways ejection is also detected in CARMA-7. In this source, a chain of small CO bow shocks is seen along the jet axis, with each bow shock associated with a spur velocity structure in the PV diagram along the jet axis (Plunkett et al. 2015, see also Fig. 9), consistent with laterally-expanding internal bow shocks. The spur structure is slightly tilted because of a small inclination of the jet to the plane of the sky.

## 7 Periodical variations and their possible origins

As discussed earlier, some of the molecular jets show roughly equal spacings in between knots and bow shocks that can be due to quasi-periodical variations in ejections, allowing us to probe quasi-periodical perturbations of the underlying accretion process in the disks. In addition, the rotating disks associated with some molecular jets are now resolved and found to have a radius smaller than 50 au (see Table 1), providing a strong constraint on the possible perturbations in the disks. Therefore, we can now further constrain the origins of the quasi-periodical variations in ejections.

The period of variation can be obtained by dividing the knot or bow shock spacing by the jet velocity. Previously in the optical jets in the later phase, at least two periods of variations, one short and one long, have been found to operate at the same time in one single jet. For example, Raga et al. (2002) found two periods of 270 yr and 1400 yr in HH 34, and two periods of 60 yr and 950 yr in HH 111. Similarly in the molecular jet HH 212 in the early phase, Zinnecker et al. (1998) also found two periods, one for the inner knots with a spacing of  $\sim 1700$  au and the other for the prominent bow shocks



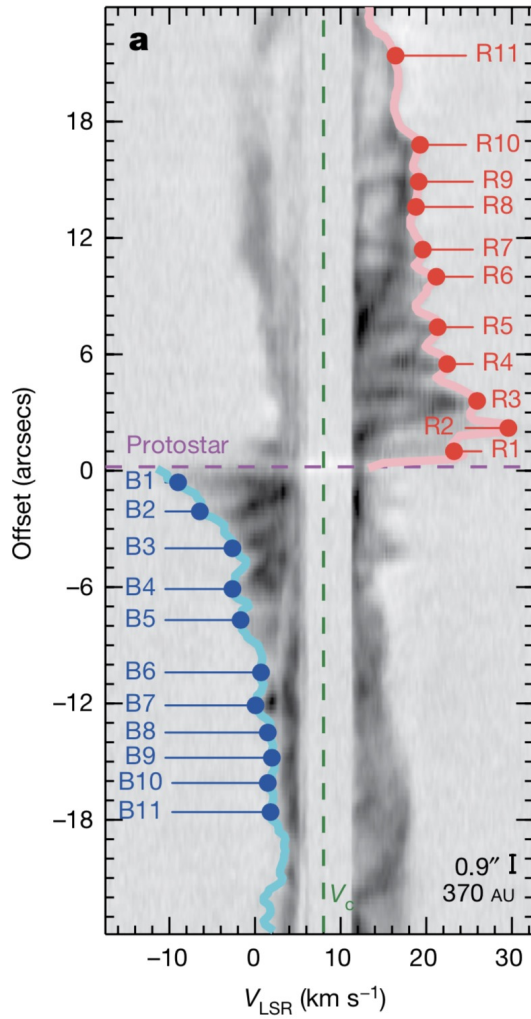


**Fig. 9** Position-velocity diagram of the CO jet in CARMA-7 along the jet axis (Plunkett et al. 2015). Labels B1 to B11 and R1 to R11 mark the positions of the internal knots and bow shocks.

with a spacing of  $\sim 17200$  au (see Figure 10). Adopting a mean jet velocity of  $\sim 135$   $\text{km s}^{-1}$  (see Table 1), these spacings correspond to periods of 60 yrs and 605 yrs, respectively. In recent high-resolution ALMA observations, an additional knot spacing of  $\sim 30$  au (see Fig. 7) with a corresponding period of  $\sim 1$  yr is also detected near the jet source. Such a short period of variation was also detected before in, e.g., the DG Tau jet which has a period of  $\sim 2.5$  yr (Agra-Amboage et al. 2011). It is believed that such a short period of variation will be found in more jets near the central sources when more high-resolution observations are obtained.

**Table 2** Periodical variations in well-defined molecular jets

Source	Spacing (au)	Period (yr)	a (au)	References
IRAS 04166+2706	1065	83	?	1
	5330	415	?	1
NGC1333 IRAS4A2	1600	76	9	2
L1157	15000	660	26	3
HH 211	256	12	2	4
	800	38	5	4
L1448 C	4300	204	15	4
	680	20	3	5
	8000	240	17	5
HH 212	30	1	0.6	6
	1700	60	10	6
	17200	605	45	6

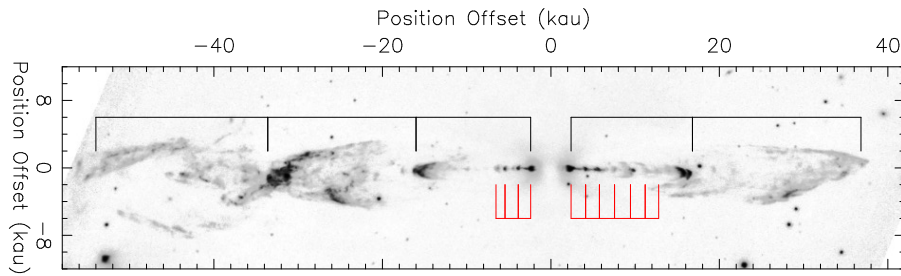
Here  $a$  is the corresponding orbital radius of the perturbation defined by Eq. 8. References: (1) [Santiago-García et al. \(2009\)](#), (2) [Choi et al. \(2011\)](#) (3) [Kwon et al. \(2015\)](#) (4) [McCaughrean et al. \(1994\)](#), [Lee et al. \(2010\)](#), (5) [Hirano et al. \(2010\)](#) (6) [Zinnecker et al. \(1998\)](#), [Lee et al. \(2017c\)](#)

Table 2 lists the periods of variations estimated from six well-defined molecular jets. These periods range from 1 yr to 660 yrs and can be broadly divided into 3 different groups: periods of a few yrs associated with knots near the jet sources, periods of a few ten yrs associated with knots and small bow shocks in the inner parts of the jets, and periods of a few hundred yrs associated with prominent bow shocks (see Fig. 10 for HH 212 and Fig. 11 for HH 211). Recent ALMA observations of a jet in the Class 0 protostar CARMA-7 show a clear chain of small CO bow shocks along the jet axis, with a spacing of  $\sim 680$  au ([Plunkett et al. 2015](#)), or a period of  $\sim 32$  yrs assuming a velocity of  $100 \text{ km s}^{-1}$ , and thus belongs to the period group of a few ten yrs. These periods could come from periodical perturbations of the underlying accretion in the disks on the orbital time scales. In order to study this possibility, we derive the corresponding orbital radii for these periods with the following equation from the Kepler's third law of orbital motion:

$$a = \left( \frac{GM_* T^2}{4\pi^2} \right)^{1/3} = \left( \frac{M_*}{M_\odot} \right)^{1/3} \left( \frac{T}{\text{yr}} \right)^{2/3} \text{ au} \quad (8)$$

where  $T$  is the period and  $M_*$  is mass of the central protostar.

As can be seen from Table 2, periods of a few hundred yrs correspond to orbital radii of a few tens of au. Interestingly in HH 212 and HH 211, the implied orbital radii of the perturbations are similar to the radii of their rotating disks, which have a radius of  $\sim 44$  and  $16$  au (see Table 1), respectively. For other jet sources, their disks are not resolved yet and further observations are needed to check this possibility. Therefore, it seems that the longest period of perturbations in the disks can come from the outer edge of the disk, probably induced by gravitational instability (GI) powered by envelope accretion. Such instability has been detected in the embedded Class I disk in HH 111, which shows a pair of spiral arms extending from the outer edge of the disk to the



**Fig. 10** Spacings between knots and major bow shocks in HH 212 seen in H<sub>2</sub> (Zinnecker et al. 1998). Red lines show the spacing for the inner knots and black lines for the prominent bow shocks.

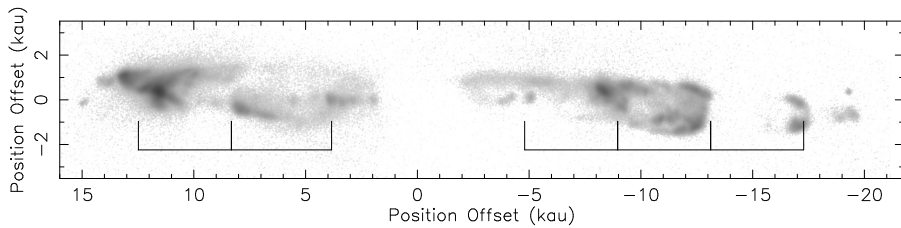


**Fig. 11** Spacing between major bow shocks in HH 211 seen in H<sub>2</sub> (Hirano et al. 2010).

inner disk where the Toomre  $Q$  parameter is of the order of unity (Lee et al. 2019b). An accretion shock is also detected around that disk in SO, indicative of an active accretion from the envelope (Lee et al. 2016). In simulations, protostellar disks could be periodically gravitationally unstable, forming spiral arms in the disks and thus producing enhanced accretion rates onto the protostars periodically (Tomida et al. 2017). These periodical enhanced accretion rates can then cause periodical major ejections (such as FU Ori-like bursts) of the jets, producing the prominent bow shocks in the jets. A recent study of a few FU Ori-type objects have detected arms and fragmented structures that can be attributed to gravitationally unstable disks (Takami et al. 2018), also supporting this possibility. In this scenario, older protostars, which have larger masses and disks, would have periods of a few thousand yrs. For example, HH 111, which has a protostellar mass of  $\sim 1.5 M_{\odot}$  and a disk radius of  $\sim 160$  au (Lee et al. 2019b), would have a period of  $\sim 1650$  yrs. HH 111 has a length of more than 10 pc (Reipurth & Bally 2001), and deeper observations in H<sub>2</sub> are needed to check for this period.

The next group of periods has a mean of  $\sim 50$  yr, with a mean corresponding orbital radius of  $\sim 6$  au. This radius could be the location where the deadzone is located with negligible ionization. One possible disturbance source is a close binary companion, which could evolve from a secondary fragmentation in a second core collapse (Machida et al. 2008). The possibility of a binary companion was also suggested in, e.g., HH 212 (Lee et al. 2007), L1448 C (Hirano et al. 2010), and HH 211 (Lee et al. 2010) because of the wiggle in their jets. Other origins could be stellar magnetic cycles or global magneto-

spheric relaxations of the star-disk system (Frank et al. 2014). Alternatively, perhaps GI can penetrate to the inner parts of the disks, forming dense (protoplanetary) clumps in spiral arms, causing enhanced accretion rates onto the protostars (Vorobyov & Basu 2005).

The shortest period is  $\sim 1$  yr in HH 212, corresponding to an orbital radius of  $\sim 0.6$  au. Similarly in the DG Tau jet, which is driven by a T-Tauri star with a mass of  $\sim 0.7 M_{\odot}$ , the corresponding orbital radius for its 2.5 yr period is  $\sim 1.5$  au (Agra-Amboage et al. 2011). It is not clear what origin can introduce this perturbation on this small orbital scale. It could be due to a periodical turn on of magneto-rotational instability (MRI) (Balbus & Hawley 2006) in the innermost parts of the disks where the temperature is high (1000 K) and the ionization is sufficient (Audard et al. 2014). It could also be related to the phase transition from dust-rich to dust-free region in the disks, because the jets are likely launched from dust-free regions in the innermost parts of the disks, as discussed later.

## 8 Wiggles and binaries?

Two types of wiggles are detected in protostellar jets in the early phase, as in the later phase. One is point-symmetric (i.e., S-shaped) wiggles that could be due to precession of the jets (e.g., Raga et al. 1993), which in turn could be due to precession of the accretion disks because of tidal interactions in noncoplanar binary systems (see, e.g., Terquem et al. 1999). The other is reflection-symmetric (i.e., C-shaped or W-type) wiggles (Fendt & Zinnecker 1998; Masciadri & Raga 2002; Lee et al. 2010; Moraghan et al. 2016) that could be due to orbital motion of the jet sources around a binary companion. Both types of wiggles can take place simultaneously in single jets (Raga et al. 2009). Unlike most of the optical jets, molecular jets are seen on both sides, allowing us to better determine the types of the wiggles and derive the binary properties. Combining with the total mass derived from other methods, we can also derive the mass of each binary component. In addition, the periods of these wiggles could be compared to those of the ejection variations in producing the knots and bow shocks in the jets, providing further constraints on the potential binary formation in the central regions of star formation in the early phase. In particular, formation of a close binary can start in the early phase before the collapse of a second core and even during the protostellar phase because of angular momentum redistribution at the center of the system (Machida et al. 2008).

The young source L1157 has a S-shaped outflow and thus a precessing jet was proposed to produce its outflow morphology (Gueth et al. 1996; Bachiller et al. 2001; Takami et al. 2011, see also Figure 12 Left). Recently, Kwon et al. (2015) proposed that there could be two precessing jets, each along one side of the outflow cavity walls, to produce the outflow morphology. However, Podio et al. (2016) detected only a single jet in SiO and CO within 200 au of the central source propagating along the symmetry axis of the outflow lobes (see

Fig. 12 Middle and Right), confirming the previously proposed one precessing jet model (Gueth et al. 1996; Bachiller et al. 2001). The precession period is  $\sim 1640$  yrs, about twice that estimated from the bow shock separation (see Table 2).

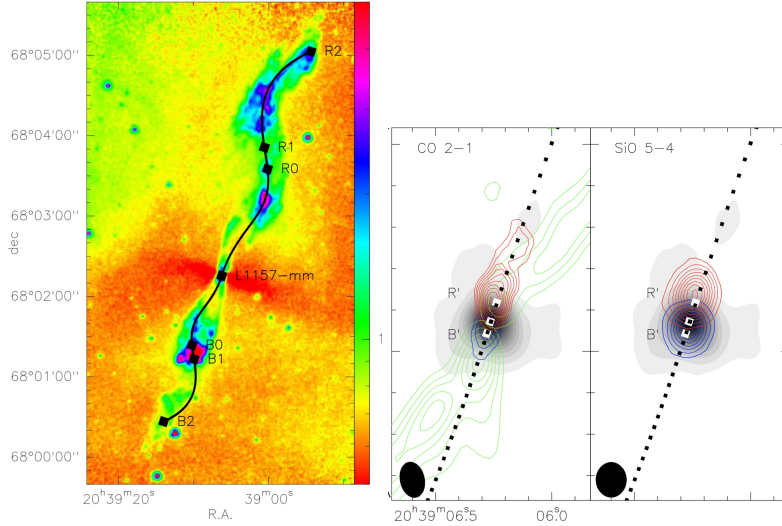


**Fig. 12** L1157 jet and outflow adopted from Podio et al. (2016). (Left) A precessing jet model plotted on the Spitzer/IRAC  $8 \mu\text{m}$  map of the outflow. (Middle) Blueshifted and redshifted CO emission of the jet. (Right) Blueshifted and redshifted SiO emission of the jet.

One mechanism to produce a precessing jet is disk precession induced by tidal interaction with a binary companion in a non-coplanar orbit (e.g., Terquem et al. 1999). The jet source has a low-mass accretion disk (with an outer radius  $r_d$ ), which is precessing as a result of the perturbations due to the companion. Let the jet source have a mass  $M_j$  and a companion a mass  $M_c$  and the binary has a separation  $a$  in a circular orbit. The ratio of precession period  $\tau_p$  to orbital period  $\tau_o$  can then be given by

$$\frac{\tau_p}{\tau_o} = \frac{32}{15 \cos \alpha} \left( \frac{a}{r_d} \right)^{3/2} \left( 1 + \frac{M_c}{M_j} \right)^{1/2} \left( \frac{M_j}{M_c} \right) \quad (9)$$

where  $\alpha$  is the half-opening angle of the resulting precession cone (Terquem et al. 1999; Anglada et al. 2007; Raga et al. 2009). Terquem et al. (1999) suggested that the tidal truncation of the accretion disk will lead to a ratio  $a/r_d = 2 - 4$ . The jet precession in L1157 could be due to this disk precession. Taking a mean ratio of  $a/r_d \sim 3$  and assuming  $M_c \sim M_j$ , we have  $\frac{\tau_p}{\tau_o} \sim 15$  and thus the orbital period  $\tau_o \sim 110$  yrs. With Equation 8, the binary separation is estimated to be  $\sim 8$  au, and thus the disk radius is  $\sim 2.7$  au. Further work is needed to check this possibility.

Another possible mechanism is an asymmetric envelope accretion onto the disk. Simulations have shown that a large misalignment between the magnetic axis and rotation axis in the star-forming core can produce a flattened infalling envelope and a rotating disk at the center. However, the major axis of the flattened infalling envelope will be misaligned with the major axis of the disk (Hirano & Machida 2019), as also seen in the observations of HH 211 (Lee et al. 2019a). In this case, the envelope accretion onto the disk will be asymmetric, causing the disk and the jet to precess (Hirano & Machida 2019). Indeed, the jet axis in HH 211 has already been found to have precessed by  $\sim 3^\circ$  in the past (Eisloffel et al. 2003), supporting this scenario.

On the other hand, reflection-symmetric wiggle has been suggested in the jets HH 211 (Lee et al. 2010; Moraghan et al. 2016) and HH 111 (Noriega-Crespo et al. 2011), and could be due to an orbital motion of the jet sources. As discussed in Masciadri & Raga (2002) and Lee et al. (2010), we can derive the period  $P_o$ , velocity  $v_o$ , and radius  $R_o$  of the orbit of the jet source around the companion from three measurable quantities: the jet velocity  $v_j$ , the half-opening angle  $\kappa$  and the periodic length (i.e., wavelength)  $\Delta z$  of the wiggle, with the following equations:

$$P_o = \frac{\Delta z}{v_j}, \quad v_o \approx \kappa v_j, \quad R_o \approx \frac{\kappa \Delta z}{2\pi} \quad (10)$$

Again, assuming the jet source has a mass  $M_j$  and the companion a mass  $M_c$ , and  $M_j = m M_c$ , then the binary separation would be  $a = (1 + m)R_o$ . From Kepler's third law of orbital motion, the total mass of the binary would be

$$M_t \approx 9.5 \times 10^{-4} (1 + m)^3 \times \left( \frac{v_j}{100 \text{ km s}^{-1}} \right)^2 \left( \frac{\kappa}{1^\circ} \right)^3 \frac{\Delta z}{100 \text{ au}} M_\odot \quad (11)$$

In HH 211, with  $\Delta z \sim 1750$  au,  $\kappa \sim 0.0094$  (or  $0.54^\circ$ ),  $v_j \sim 110$  km s $^{-1}$ , and  $M_t \sim 0.08 M_\odot$  (Lee et al. 2019a), we have  $P_o \sim 83$  yrs,  $v_o \sim 0.94$  km s $^{-1}$ ,  $R_o \sim 2.6$  au,  $m \sim 2.1$ , and  $a \sim 8.2$  au. The mass of the jet source would be  $\sim 0.053 M_\odot$ . The orbital period is  $\sim 2$  times that generates the knot separation, which is  $\sim 38$  yrs (see Table 2). It is possible that the orbit is eccentric and two perturbations could generate two knots per orbit. This could occur either through the periastron passage to the companion and a close approach to the inner edge of the circumbinary disk, or two close approaches to the inner edge of the circumbinary disk per eccentric orbit (Moraghan et al. 2016). Since the binary separation here is about half of the disk radius, observations at higher resolution are needed to resolve the binary and check this possibility. On the other hand, in HH 111, with  $\Delta z \sim 86400$  au,  $\kappa \sim 0.013$  (or  $0.74^\circ$ ), and  $v_j \sim 240$  km s $^{-1}$  (Noriega-Crespo et al. 2011), and a total mass of  $\sim 1.5 M_\odot$  (Lee 2010; Lee et al. 2016), we have  $P_o \sim 1710$  yrs,  $v_o \sim 3.1$  km s $^{-1}$ , and  $R_o \sim 178$  au,  $m \sim -0.1$ , and  $a \sim 163$  au. Thus, within the uncertainty, the jet source has almost no mass, inconsistent with it driving a powerful jet longer than 10 pc (Reipurth & Bally 2001). In addition, the

binary separation would be similar to the disk radius, which is  $\sim 160$  au (Lee et al. 2019b), but no binary companion was detected there around the edge of the disk (Lee et al. 2019b). Thus, further work is needed to check the reflection-symmetric wiggle in the HH 111 jet.

## 9 Magnetic fields in the jets

For high-mass protostars, synchrotron radiation have been detected in a few protostellar jets, e.g., HH 80-81 (Marti et al. 1993) and W3(OH) (Wilner et al. 1999), at centimeter wavelengths, indicating a presence of magnetic fields in the jets. Magnetic field morphology can thus be derived from the polarization pattern of the synchrotron radiation. So far, polarization has only been detected in HH 80-81 (Carrasco-González et al. 2010). It was detected at a spatial resolution of  $\sim 20,000$  au towards the jetlike structures at a large ( $\gtrsim 30,000$  au) distance from the central protostar, where the underlying jet interacts with the ambient material (Rodríguez-Kamenetzky et al. 2017). The implied magnetic fields there are mainly poloidal, with a field strength of  $\sim 0.2$  mG. There is also a hint of toroidal fields near the edges of the jetlike structures. However, more sensitive observations are needed to detect the polarized emission and thus the field morphology in the underlying jet itself, which is much narrower with a radius of  $\sim 2000$  au (Rodríguez-Kamenetzky et al. 2017). Recent observations in W3(H<sub>2</sub>O) (Goddi et al. 2017) also detected linear and circular polarizations in the water masers at the center of the synchrotron jet within tens to hundreds of au from the central source. They suggested that the magnetic field could evolve from having a dominant component parallel to the outflow velocity in the pre-shock gas, with field strengths of a few tens of mG, to being mainly dominated by the perpendicular component of a few hundred of mG in the post-shock gas where the H<sub>2</sub>O masers are excited.

For low-mass protostars, the jets are less energetic and thus do not have strong enough synchrotron radiation and water masers for polarization detection with current instruments. Fortunately, when they are young, they have a high content of molecular gas because of high mass-loss rate (Glassgold et al. 1991; Shang et al. 2006; Cabrit et al. 2007; Lee et al. 2007; Hirano et al. 2010), allowing us to map their magnetic fields using the linear polarization in molecular lines with the so-called Goldreich–Kylafis (GK) effect (Goldreich & Kylafis 1981, 1982). In the presence of a magnetic field, a molecular rotational level splits into magnetic sublevels, producing a line polarization with its orientation either parallel or perpendicular to the magnetic field. Recent successful detection of this GK effect in the SiO line in HH 211 confirmed this method of mapping the field morphology in the jets from the low-mass protostars (Lee et al. 2018c). In the future, sensitive observations of the Zeeman effect in molecular lines will allow us to derive the strength of the magnetic fields (Cazzoli et al. 2017).

Figure 13 shows the SiO line polarization in J=8-7 transition detected in the HH 211 jet within a few hundred au of the protostar. The jet is best

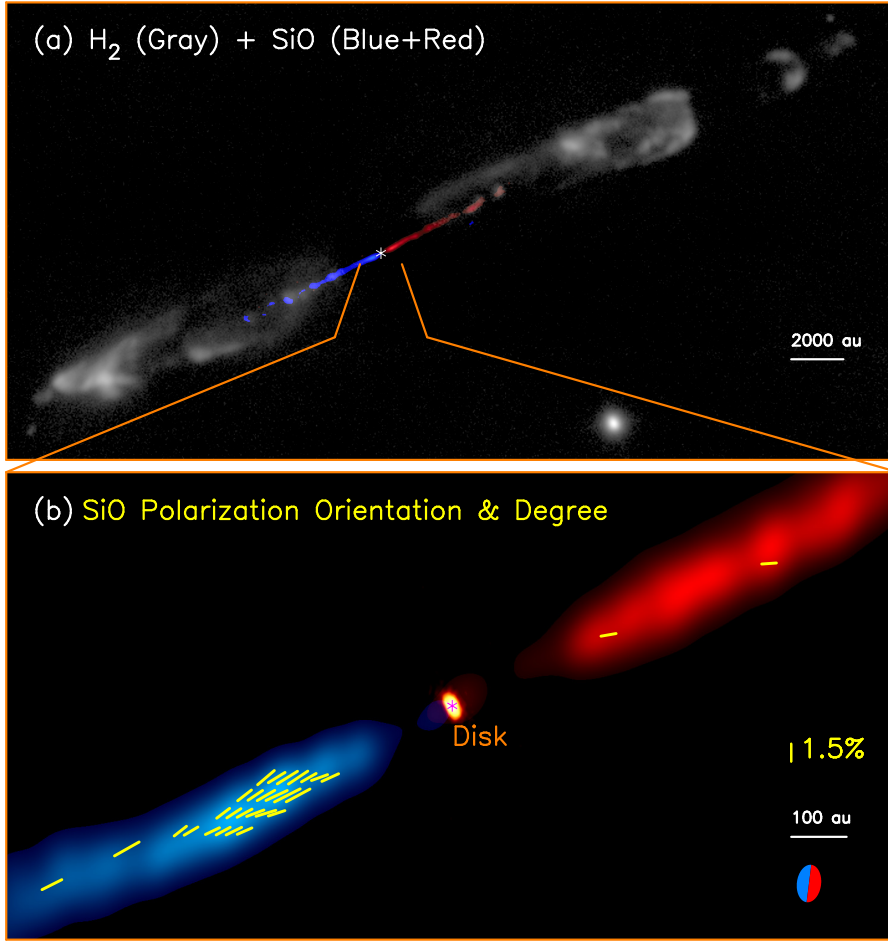


**Fig. 13** SiO J=8-7 line polarization detection in the HH 211 jet (Lee et al. 2018c). The asterisk marks the position of the central driving source. Gray image shows the outflow and the outer part of the jet in H<sub>2</sub> adopted from Hirano et al. (2006). Blue image and red image show the blueshifted and redshifted jet components in SiO, respectively. Yellow line segments indicate the polarization orientations seen in SiO.

seen in SiO in the J=8-7 transition. At this transition, the optical depth is close to 1 (Lee et al. 2009) and the collision rate is lower than the radiative transition rate for a typical jet density of  $10^6$ – $10^7$  cm<sup>-3</sup>, both optimal for polarization from the GK effect (Goldreich & Kylafis 1981, 1982). As can be seen, the polarization orientations are all roughly parallel to the jet axis. The implied magnetic fields could be either mainly poloidal or mainly toroidal and additional polarization observations in another SiO transition line are needed to resolve this ambiguity in the field morphology, as done before in a CO outflow (Ching et al. 2016). It could be mainly toroidal, as suggested in current jet-launching models, in order to collimate the jet at large distances.



The field strength (projected on the plane of the sky) was estimated to be  $\sim 15$  mG (Lee et al. 2018c). This field strength is about 2 times the toroidal field strength expected from a typical X-wind model (Shu et al. 1995) for a low-mass protostellar jet like HH 211, which is reasonable considering a shock compression in the jet and all the uncertainties in the measurements.

The jets may have poloidal fields as well. In HH 212, the jet is found to be wiggling, but with the amplitude of the wiggle being saturated at some distance, inconsistent with a typical jet precession that has an amplitude increasing linearly with the distance. The saturation in the amplitude may suggest a current-driven kink instability in the jet (Cerqueira & de Gouveia Dal Pino 2001), see, e.g., Fig. 3 in both Cerqueira & de Gouveia Dal Pino (2001) and Mizuno et al. (2014). For the kink instability to take place, we have the Kruskal–Shafranov criterion  $|B_p/B_\phi| < \lambda/2\pi A_m$  (e.g., Bateman 1978), where  $A_m$  is the maximum displacement and  $\lambda$  is the wiggle wavelength. In HH 212, with  $A_m \sim 0''.1$  and  $\lambda \sim 5''.6$ , we have  $|B_p/B_\phi| < 9$ . Therefore, this kink instability, if in action, could be initiated in the central part of the jet, where the magnetic field is dominated by the poloidal field (Pudritz et al. 2012). This poloidal field could serve as a “backbone” to stabilize the jet (Ouyed et al. 2003). The toroidal field dominates only near the jet edges in order to collimate the jet.

## 10 Origin of molecular gas in the jets

Unlike those in the Class I and Class II phases, the jets in the Class 0 phase appear to be mainly molecular and well detected in CO, SiO, and SO. Note that near the base of the jets, free-free emission from ionic gas can also be detected in the Class 0 phase (Rodríguez 1997; Reipurth et al. 2002, 2004; Rodríguez et al. 2014; Tobin et al. 2016). It is possible that the high molecular content in the Class 0 phase is due to the high mass-loss rate and thus the fast formation rate of the molecular gas. Since the mass-loss rate in the jets is high ( $\sim 10^{-6} M_\odot \text{ yr}^{-1}$ ), molecules such as CO, SiO, and SO could have formed via gas-phase reactions in an initially atomic jet close to the launching point within 0.1 au (Glassgold et al. 1991). The abundances of SiO and SO in the gas phase are found to be highly enhanced in the jets as compared to those in the quiescent molecular clouds, even close to within 30 au of the central sources where the dynamical timescale is  $< 1$  yr (Lee et al. 2017c, 2018a; Bjerkeli et al. 2019).

As discussed earlier, based on the ejection efficiency, jet rotation, and the expansion of jet radius near the jet sources, the molecular jets in the Class 0 phase should be launched within  $\sim 0.1$  au of the jet sources. Most of these jet sources have a bolometric luminosity  $\gtrsim 1 L_\odot$ , suggesting that the dust sublimation radius in their accretion disks is  $\gtrsim 0.1$  au (Millan-Gabet et al. 2007), which is outside the inferred jet launching radius. In the case of HH 212, Tabone et al. (2017) proposed that the SiO jet could be the innermost part of a disk wind launched at  $\sim 0.05$ – $0.2$  au, by modeling the PV structures

of the SiO emission across the jet axis (see their Figs. 2e and 2f). Since their model PV structures show emission peaks at the two high-velocity ends instead of at the low velocity on the jet axis, the major part of the jet must still be launched significantly closer than 0.2 au. In any case, since the jet source in HH 212 has a bolometric luminosity of  $9 L_{\odot}$ , the sublimation radius should be  $\sim 0.2$  au (Millan-Gabet et al. 2007), and thus still larger than the launching radius.

It is likely that elements such as Si, S, C, and O, are already released from the grains into the gas phase at the base of the jets. Since the jets are well collimated with a high mass-loss rate of  $\sim 10^{-6} M_{\odot} \text{ yr}^{-1}$  (see Table 1), SiO, CO, and SO can form quickly within  $\sim 0.1$  au because of the high density in the jet (Glassgold et al. 1991). The jets are bright in SiO J=8-7, which has a high critical density of  $\gtrsim 10^7 \text{ cm}^{-3}$ , further supporting the high density in the jets. In addition, the  $\text{Si}^+$  recombination and SiO formation are expected to be faster than the photodissociation caused by possible far-ultraviolet radiation of the central protostar (Cabrit et al. 2012). Since these molecules are fully released from the dust grains at the base, the observed abundances in the jets are higher as compared to those in the quiescent molecular clouds.

For the jet sources with a bolometric luminosity  $< 1 L_{\odot}$ , e.g., B335 and IRAS 04166+2706 (see Table 1), the dust sublimation radius is  $< 0.1$  au (Millan-Gabet et al. 2007). However, it is still possible that their jets are launched from a dust-free zone, because their jet launching radius could be smaller, as discussed earlier. In B335, since the mass-loss rate is only  $\sim 10^{-7} M_{\odot} \text{ yr}^{-1}$ , further work is needed to check if the density in the jet is high enough to form the molecules in the gas phase. In this source, the SiO J=5-4 emission is only detected within a few au of the jet source, probably because the mass-loss rate is low.

In case the jets are launched from dusty zones, SiO abundance in the jets can be enhanced as a consequence of grain sputtering or grain-grain collisions in the shocks releasing Si-bearing material into the gas phase, which reacts rapidly with O-bearing species (e.g.,  $\text{O}_2$  and OH) to form SiO (Schilke et al. 1997; Caselli et al. 1997). Another possible explanation is that the SiO molecules existed on the grain mantles and are released into the gas phase by means of shocks as suggested by Gusdorf et al. (2008). Similarly, sulfur can be released from dust grains in the form of  $\text{H}_2\text{S}$  in the shocks and that is then oxidized to SO (Bachiller et al. 2001). Alternatively, the SO molecules might be abundant on dust grains and directly released from grains in the shocks (Jiménez-Serra et al. 2005; Podio et al. 2015).

## 11 Disk winds around the jets?

As discussed earlier, protostellar jets can carry angular momentum away from the innermost region of the disks, allowing the disk material to feed the central protostars. However, other mechanisms are also needed to transfer angular momentum outward within the disks or carry it away from the disks, so that

the disk material can be transported to the innermost region from the outer region of the disks. For example, MRI can turn on in the inner part of the disks where the temperature is high ( $\gtrsim 1000$  K) (Audard et al. 2014) to transfer angular momentum outward. GI can also be excited in the outer part of the disks to transfer angular momentum outward, as suggested in many simulations (Bate 1998; Tomida et al. 2017) and by the detections of a pair of spirals in the embedded disk in HH 111 (Lee et al. 2019b) and probably in the older disk in Elias 2-26 (Pérez et al. 2016). Besides, low-velocity extended tenuous disk winds can be present as well to carry angular momentum away from the disks. In particular, previous observations have shown that wide-angle radial winds are needed to drive molecular outflows (Lee et al. 2000, 2001; Hirano et al. 2010; Arce et al. 2013), especially in the later phase of star formation (Lee & Ho 2005).

In the two popular magneto-centrifugal jet-launching models from the disks, e.g., the X-wind model and the disk-wind model, the jets are merely the central cores of the winds. Therefore, in addition to the jets, the models also predict wide-angle tenuous winds around the jets. In the X-wind model, the wide-angle wind comes from the same disk radius as the jet within  $\sim 0.05$  au of the central source. This model has been proposed to produce the molecular outflows and the collimated jets simultaneously (Shang et al. 2006). On the other hand, in the disk-wind model, an extended (wide-angle) disk wind comes from a range of radii up to  $\sim 20$  au around the central jet, extracting angular momentum from the disks at larger radii. The detections of poorly collimated and low-velocity rotating molecular outflows near the disks in a few older sources, including CB 26 (Class II) (Launhardt et al. 2009), TMC1A (Class I) (Bjerkeli et al. 2016), and HH 30 (Class II) (Louvet et al. 2018), strongly support this possibility. For example, in TMC1A, a low-velocity and poorly collimated CO outflow was proposed to be driven by an extended disk wind coming from the disk surface with a radius up to 25 au from the central source. A poorly collimated and low-velocity rotating molecular outflow was also detected in the high-mass source Orion BN/KL Source I (Greenhill et al. 2013; Hirota et al. 2017) and it can also be driven by an extended disk wind coming from the disk surface with a radius up to  $\sim 20$  au from the central source. Nonetheless, further works are still needed to check if the rotating outflows can also be rotating envelope material swept up by inner winds, either the wide-angle components of X-winds or the inner disk winds.

In the early phase, disk winds could also be present around the molecular jets, e.g., in HH 212 (Tabone et al. 2017; Lee et al. 2018a) and HH 211 (Lee et al. 2018b). For example, in HH 212, by modeling a rotating SO outflow near the disk around the jet, Tabone et al. (2017) suggested that the outflow can trace a wind coming from the disk at a radius up to 40 au to the outer edge of the disk, as shown in the schematic diagram in Figure 14. The disk wind could be massive and can carry away  $\sim 50\%$  of the incoming accretion flow (Tabone et al. 2017). This SO outflow was later observed and resolved at higher angular resolution, and found to extend out to only  $\sim 70$  au above and below the disk midplane (Lee et al. 2018a, see also Fig. 15). It has a specific

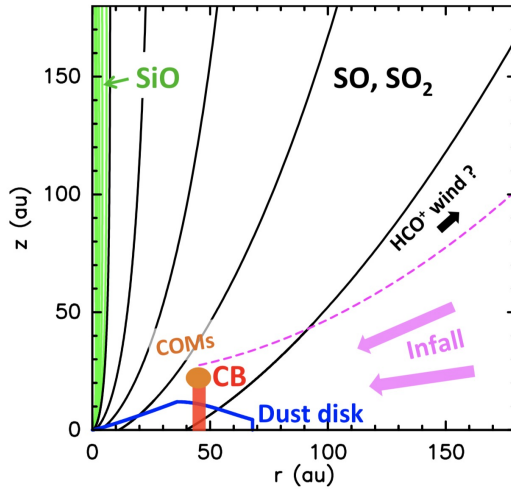


**Fig. 14** Schematic view of the inner 180 au region of the HH212 system, showing the SiO jet and a possible SO disk wind around the jet (Tabone et al. 2017). Here CB means centrifugal barrier and COMs means complex organic molecules in the disk atmosphere.

angular momentum of  $\lesssim 40 \text{ au km s}^{-1}$ , indicating that it could trace a disk wind launched at a radius up to  $\sim 7 \text{ au}$  (Lee et al. 2018a). However, further observations are needed to check if the rotating SO outflow could also trace the material in the rotating disk atmosphere being pushed up and out by an inner wind launched at the innermost disk, e.g., a wide-angle radial wind component surrounding the fast jet as in the X-wind model.

## 12 Summaries and conclusions

Recent results of a small sample of molecular jets at high spatial and velocity resolution have provided strong constraints on jet launching and collimation. The mean ratio of the mass-loss rate in the jet to the accretion rate is  $\sim 0.2$ , as expected in magneto-centrifugal jet-launching models. This ratio implies a magnetic lever arm parameter of  $\sim 5$  and a jet launching radius of  $\sim 0.04 \text{ au}$ . More importantly, a clear rotation is detected in the HH 212 jet within 100 au of the central source, with a rotation sense the same as that of the disk, confirming the role of the jet in removing angular momentum from the disk. The specific angular momentum of the jet is  $\sim 10 \text{ au km s}^{-1}$ , consistent with the jet being launched from the innermost edge of the disk at  $\sim 0.04 \text{ au}$ . The jet is expanding roughly with the square of the distance from the central source, roughly consistent with that predicted in magneto-centrifugal jet-launching models, where the jet is collimated internally by its own toroidal magnetic field. There is also a hint of a hollow cone in this jet, because the knots in this jet show a linear velocity structure that can come from a ring. Assuming

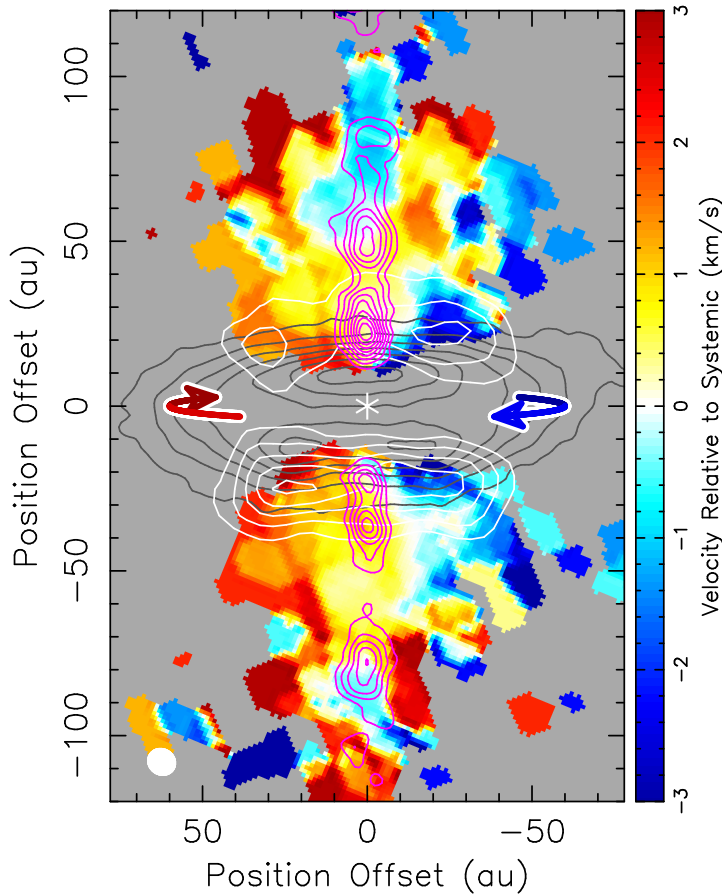


**Fig. 15** SO rotating outflow from the disk around the SiO jet in HH 212 (Lee et al. 2018a). Magenta contours show the SiO jet. Gray contours show the continuum map of the disk at  $850 \mu\text{m}$ . White contours show the disk atmosphere detected in  $\text{CH}_2\text{DOH}$ . Color maps show the intensity-weighted velocity of the SO outflow. The red and blue arrows show the rotation of the disk.

that the knots are indeed rings, then the knots have a radius slightly larger than that of a hollow cone with a launching radius of  $\sim 0.04$  au, consistent with the jet tracing the innermost core of the wind in the magneto-centrifugal jet-launching models.

The knots and bow shocks in the jets likely trace the internal shocks produced by quasi-periodical variations in ejection velocity, which in turn is induced by quasi-periodical perturbations of the accretion in the disks. Sideways ejections are detected in the knots and bow shocks. Nested internal shells are also detected, with each extending from a bow shock back to the central source. Up to 3 periodical variations are detected in the jets, with one having a period of a few yrs, one with a period of a few ten yrs, and one with a period of a few hundred yrs. The one with a period of a few hundred yr could be in-

duced by gravitational instability powered by envelope accretion. Others could be due to binary companions, either stellar or planetary, magneto-rotational instabilities, gravitational instability penetrating to the inner disks, etc.

Two types of wiggles, point-symmetric and reflection-symmetric, are detected in the jet trajectories. The point-symmetric wiggle could be due to jet precession, which in turn could be due to disk precession. Disk precession can be induced by tidal interactions in noncoplanar binary systems. It can also be induced by asymmetric envelope accretion, when there is a misalignment between the flattened envelope and the disk because of a misalignment between the magnetic axis and rotation axis in the star-forming core. On the other hand, the reflection-symmetric wiggle could be due to an orbital motion of the jet sources around the binary companions.

High sensitivity observations with ALMA can detect SiO line polarization in molecular jets due to the Goldreich–Kylafis effect, allowing us to map the magnetic field morphology in the jets. Recently, SiO line polarization has been detected toward a well-defined jet within a few hundred au of the central source, with an orientation parallel to the jet axis, indicating that the magnetic field there could be either mainly toroidal or mainly poloidal. Additional polarization observations in SiO in different line transitions are needed to resolve the ambiguity in the field morphology. Moreover, current-driven kink instability might have been detected in one of the jets, suggesting a possible presence of a poloidal field in the jet core as well.

Being launched within a radius  $< 0.1$  au of the central sources, molecular jets are likely launched from dust-free regions. The high content of molecular gas in the jets likely arise because the mass-loss rate is high  $\sim 10^{-6} M_{\odot} \text{ yr}^{-1}$ , so that molecules can form quickly in the jets. Current observations show that a SiO jet can be detected down to within  $\sim 3$  au of the central source, where the dynamical age is less than a month, strongly supporting this possibility.

Rotating molecular outflows are detected around a few molecular jets, suggestive of a presence of extended disk winds around the jets. The extended disk winds are expected to carry angular momentum away from the disks, allowing the disk material to be transported to the inner parts from the outer parts. However, more works are needed to check if the rotating outflows can also be rotating envelope material or disk atmosphere swept up by inner winds, either the wide-angle components of the X-winds or the inner disk winds.

In summary, recent observations of a small sample of molecular jets have opened up opportunities for us to detect the jet rotation, to resolve the jet structure and search for a hollow cone, to map the magnetic field, to study the periodical variation in ejection and thus the periodical perturbations in disk accretion, etc. Future systematic observations with a large sample of molecular jets at high spatial and velocity resolution with ALMA are expected to lead to a breakthrough understanding in the study of jets. In addition, sensitive observations of the Zeeman effect in molecular lines will allow us to derive the strength of the magnetic fields in the jets.

**Acknowledgements** C.-F.L. acknowledges grants from the Ministry of Science and Technology of Taiwan (MoST 107-2119-M-001-040-MY3) and the Academia Sinica (Investigator Award). I thank the referee Bo Reipurth for his carefully reading my manuscript and for his useful comments and suggestions. I also thank Anthony Moraghan for his helpful suggestions on English grammar.

## References

- Agra-Amboage V., Dougados C., Cabrit S., Reunanen J. (2011) Sub-arcsecond [Fe ii] spectro-imaging of the DG Tauri jet. Periodic bubbles and a dusty disk wind?. *A&A*, 532:A59. <https://doi.org/10.1051/0004-6361/201015886>
- Anderson J. M., Li Z.-Y., Krasnopolsky R., Blandford R. D. (2003) Locating the Launching Region of T Tauri Winds: The Case of DG Tauri. *ApJ*, 590:L107-L110. <https://doi.org/10.1086/376824>
- Anglada G., López R., Estalella R., Masegosa J., Riera A., Raga A. C. (2007) Proper Motions of the Jets in the Region of HH 30 and HL/XZ Tau: Evidence for a Binary Exciting Source of the HH 30 Jet. *AJ*, 133:2799-2814. <https://doi.org/10.1086/517493>
- Anglada G., Rodríguez L. F., Carrasco-González C. (2018) Radio jets from young stellar objects. *A&A Rev.*, 26:3. <https://doi.org/10.1007/s00159-018-0107-z>
- Arce H. G., Mardones D., Corder S. A., Garay G., Noriega-Crespo A., Raga A. C. (2013) ALMA Observations of the HH 46/47 Molecular Outflow. *ApJ*, 774:39. <https://doi.org/10.1088/0004-637X/774/1/39>
- Arce H. G., Shepherd D., Gueth F., Lee C.-F., Bachiller R., Rosen A., Beuther H. (2007) Molecular Outflows in Low- and High-Mass Star-forming Regions. *Protostars and Planets V*:245. <https://doi.org/>
- Audard M., Ábrahám P., Dunham M. M., et al. (2014) Episodic Accretion in Young Stars. *Protostars and Planets VI*:387. [https://doi.org/10.2458/azu\\_uapress\\_9780816531240-ch017](https://doi.org/10.2458/azu_uapress_9780816531240-ch017)
- Bacciotti F., Ray T. P., Mundt R., Eisloffel J., Solf J. (2002) Hubble Space Telescope/STIS Spectroscopy of the Optical Outflow from DG Tauri: Indications for Rotation in the Initial Jet Channel. *ApJ*, 576:222-231. <https://doi.org/10.1086/341725>
- Bachiller R., Pérez Gutiérrez M., Kumar M. S. N., Tafalla M. (2001) Chemically active outflow L 1157. *A&A*, 372:899-912. <https://doi.org/10.1051/0004-6361:20010519>
- Balbus S. A., Hawley J. F. (2006) An Exact, Three-dimensional, Time-dependent Wave Solution in Local Keplerian Flow. *ApJ*, 652:1020-1027. <https://doi.org/10.1086/508320>
- Bally J. (2016) Protostellar Outflows. *ARA&A*, 54:491-528. <https://doi.org/10.1146/annurev-astro-081915-023341>
- Bate M. R. (1998) Collapse of a Molecular Cloud Core to Stellar Densities: The First Three-dimensional Calculations. *ApJ*, 508:L95-L98. <https://doi.org/10.1086/311719>
- Bateman, G. 1978, *MHD Instabilities* (Cambridge, MA: MIT Press)
- Benisty M., Perraut K., Mourard D., et al. (2013) Enhanced  $H\alpha$  activity at periastron in the young and massive spectroscopic binary HD 200775. *A&A*, 555:A113. <https://doi.org/10.1051/0004-6361/201219893>
- Bjerkeli P., van der Wiel M. H. D., Harsono D., Ramsey J. P., Jørgensen J. K. (2016) Resolved images of a protostellar outflow driven by an extended disk wind. *Nature*, 540:406-409. <https://doi.org/10.1038/nature20600>
- Bjerkeli P., Ramsey J. P., Harsono D., Calcutt H., Kristensen L. E., van der Wiel M. H. D., Jørgensen J. K., Muller S., Persson M. V. (2019) Kinematics around the B335 protostar down to au scales. *A&A*, 631:A64. <https://doi.org/10.1051/0004-6361/201935948>
- Cabrit S., Codella C., Gueth F., Nisini B., Gusdorf A., Dougados C., Bacciotti F. (2007) PdBI sub-arcsecond study of the SiO microjet in HH212. Origin and collimation of class 0 jets. *A&A*, 468:L29-L32. <https://doi.org/10.1051/0004-6361:20077387>
- Cabrit S., Codella C., Gueth F., Gusdorf A. (2012) High SiO abundance in the HH212 protostellar jet. *A&A*, 548:L2. <https://doi.org/10.1051/0004-6361/201219784>

- Caratti o Garatti A., Stecklum B., Linz H., Garcia Lopez R., Sanna A. (2015) A near-infrared spectroscopic survey of massive jets towards extended green objects. *A&A*, 573:A82. <https://doi.org/10.1051/0004-6361/201423992>
- Carrasco-González C., Rodríguez L. F., Anglada G., Martí J., Torrelles J. M., Osorio M. (2010) A Magnetized Jet from a Massive Protostar. *Science*, 330:1209. <https://doi.org/10.1126/science.1195589>
- Caselli P., Hartquist T. W., Havnes O. (1997) Grain-grain collisions and sputtering in oblique C-type shocks. *A&A*, 322:296-301. <https://doi.org/>
- Cazzoli G., Lattanzi V., Coriani S., Gauss J., Codella C., Ramos A. A., Cernicharo J., Puzzarini C. (2017) Zeeman effect in sulfur monoxide. A tool to probe magnetic fields in star forming regions. *A&A*, 605:A20. <https://doi.org/10.1051/0004-6361/201730858>
- Cerqueira A. H., de Gouveia Dal Pino E. M. (2001) Three-dimensional Magnetohydrodynamic Simulations of Radiatively Cooling, Pulsed Jets. *ApJ*, 560:779-791. <https://doi.org/10.1086/322245>
- Ching T.-C., Lai S.-P., Zhang Q., Yang L., Girart J. M., Rao R. (2016) Helical Magnetic Fields in the NGC 1333 IRAS 4A Protostellar Outflows. *ApJ*, 819:159. <https://doi.org/10.3847/0004-637X/819/2/159>
- Choi M., Hodapp K. W., Hayashi M., Motohara K., Pak S., Pyo T.-S. (2006) Variability of the NGC 1333 IRAS 4A Outflow: Molecular Hydrogen and Silicon Monoxide Images. *ApJ*, 646:1050-1058. <https://doi.org/10.1086/505037>
- Choi M., Tatematsu K., Kang M. (2010) Kinematics of the Ammonia Disk Around the Protostar NGC 1333 IRAS 4A2. *ApJ*, 723:L34-L37. <https://doi.org/10.1088/2041-8205/723/1/L34>
- Choi M., Kang M., Tatematsu K. (2011) Rotation of the NGC 1333 IRAS 4A2 Protostellar Jet. *ApJ*, 728:L34. <https://doi.org/10.1088/2041-8205/728/2/L34>
- Chrysostomou A., Bacciotti F., Nisini B., Ray T. P., Eisloffel J., Davis C. J., Takami M. (2008) Investigating the transport of angular momentum from young stellar objects. Do H2 jets from class I YSOs rotate?. *A&A*, 482:575-583. <https://doi.org/10.1051/0004-6361:20078494>
- Codella C., Cabrit S., Gueth F., Cesaroni R., Bacciotti F., Lefloch B., McCaughrean M. J. (2007) A highly-collimated SiO jet in the HH212 protostellar outflow. *A&A*, 462:L53-L56. <https://doi.org/10.1051/0004-6361:20066800>
- Codella C., Maury A. J., Gueth F., Maret S., Belloche A., Cabrit S., André P. (2014) First results from the CALYPSO IRAM-PdBI survey. III. Monopolar jets driven by a protobinary system in NGC 1333-IRAS2A. *A&A*, 563:L3. <https://doi.org/10.1051/0004-6361/201323024>
- Coffey D., Bacciotti F., Ray T. P., Eisloffel J., Woitas J. (2007) Further Indications of Jet Rotation in New Ultraviolet and Optical Hubble Space Telescope STIS Spectra. *ApJ*, 663:350-364. <https://doi.org/10.1086/518100>
- Coffey D., Rigliaco E., Bacciotti F., Ray T. P., Eisloffel J. (2012) Jet Rotation Investigated in the Near-ultraviolet with the Hubble Space Telescope Imaging Spectrograph. *ApJ*, 749:139. <https://doi.org/10.1088/0004-637X/749/2/139>
- Eisloffel J., Froebrich D., Stanke T., McCaughrean M. J. (2003) Molecular Outflows in the Young Open Cluster IC 348. *ApJ*, 595:259-265. <https://doi.org/10.1086/377216>
- Ellerbroek L. E., Podio L., Kaper L., Sana H., Huppenkothen D., de Koter A., Monaco L. (2013) The outflow history of two Herbig-Haro jets in RCW 36: HH 1042 and HH 1043. *A&A*, 551:A5. <https://doi.org/10.1051/0004-6361/201220635>
- Evans N. J., Dunham M. M., Jørgensen J. K., et al. (2009) The Spitzer c2d Legacy Results: Star-Formation Rates and Efficiencies; Evolution and Lifetimes. *ApJS*, 181:321-350. <https://doi.org/10.1088/0067-0049/181/2/321>
- Fendt C., Zinnecker H. (1998) Possible bending mechanisms of protostellar jets. *A&A*, 334:750-755. <https://doi.org/>
- Frank A., Ray T. P., Cabrit S., et al. (2014) Jets and Outflows from Star to Cloud: Observations Confront Theory. *Protostars and Planets VI*:451. [https://doi.org/10.2458/azu\\_uapress\\_9780816531240-ch020](https://doi.org/10.2458/azu_uapress_9780816531240-ch020)
- Froebrich D. (2005) Which Are the Youngest Protostars? Determining Properties of Confirmed and Candidate Class 0 Sources by Broadband Photometry. *ApJS*, 156:169-177. <https://doi.org/10.1086/426441>



- Glassgold A. E., Mamon G. A., Huggins P. J. (1991) The Formation of Molecules in Protostellar Winds. *ApJ*, 373:254. <https://doi.org/10.1086/170045>
- Goddi C., Surcis G., Moscadelli L., Imai H., Vlemmings W. H. T., van Langevelde H. J., Sanna A. (2017) Measuring magnetic fields from water masers in the synchrotron protostellar jet in W3(H<sub>2</sub>O). *A&A*, 597:A43. <https://doi.org/10.1051/0004-6361/201629321>
- Goldreich P., Kylafis N. D. (1981) On mapping the magnetic field direction in molecular clouds by polarization measurements. *ApJ*, 243:L75-L78. <https://doi.org/10.1086/183446>
- Goldreich P., Kylafis N. D. (1982) Linear polarization of radio frequency lines in molecular clouds and circumstellar envelopes. *ApJ*, 253:606-621. <https://doi.org/10.1086/159663>
- Green J. D., Evans N. J., Jørgensen J. K., et al. (2013) Embedded Protostars in the Dust, Ice, and Gas In Time (DIGIT) Herschel Key Program: Continuum SEDs, and an Inventory of Characteristic Far-infrared Lines from PACS Spectroscopy. *ApJ*, 770:123. <https://doi.org/10.1088/0004-637X/770/2/123>
- Greenhill L. J., Goddi C., Chandler C. J., Matthews L. D., Humphreys E. M. L. (2013) Dynamical Evidence for a Magnetocentrifugal Wind from a 20 M<sub>⊙</sub> Binary Young Stellar Object. *ApJ*, 770:L32. <https://doi.org/10.1088/2041-8205/770/2/L32>
- Gueth F., Guilloteau S., Bachiller R. (1996) A precessing jet in the L1157 molecular outflow.. *A&A*, 307:891-897. <https://doi.org/>
- Gueth F., Guilloteau S., Bachiller R. (1998) SiO shocks in the L1157 molecular outflow. *A&A*, 333:287-297. <https://doi.org/>
- Gueth F., Guilloteau S. (1999) The jet-driven molecular outflow of HH 211. *A&A*, 343:571-584. <https://doi.org/>
- Gusdorf A., Pineau Des Forêts G., Cabrit S., Flower D. R. (2008) SiO line emission from interstellar jets and outflows: silicon-containing mantles and non-stationary shock waves. *A&A*, 490:695-706. <https://doi.org/10.1051/0004-6361:200810443>
- Hartigan P., Heathcote S., Morse J. A., Reipurth B., Bally J. (2005) Proper Motions of the HH 47 Jet Observed with the Hubble Space Telescope. *AJ*, 130:2197-2205. <https://doi.org/10.1086/491673>
- Hartigan P., Frank A., Foster J. M., Wilde B. H., Douglas M., Rosen P. A., Coker R. F., Blue B. E., Hansen J. F. (2011) Fluid Dynamics of Stellar Jets in Real Time: Third Epoch Hubble Space Telescope Images of HH 1, HH 34, and HH 47. *ApJ*, 736:29. <https://doi.org/10.1088/0004-637X/736/1/29>
- Hirano N., Liu S.-Y., Shang H., Ho P. T. P., Huang H.-C., Kuan Y.-J., McCaughrean M. J., Zhang Q. (2006) SiO J = 5-4 in the HH 211 Protostellar Jet Imaged with the Submillimeter Array. *ApJ*, 636:L141-L144. <https://doi.org/10.1086/500201>
- Hirano N., Ho P. T. P., Liu S.-Y., Shang H., Lee C.-F., Bourke T. L. (2010) Extreme Active Molecular Jets in L1448C. *ApJ*, 717:58-73. <https://doi.org/10.1088/0004-637X/717/1/58>
- Hirano S., Machida M. N. (2019) Origin of misalignments: protostellar jet, outflow, circumstellar disc, and magnetic field. *MNRAS*, 485:4667-4674. <https://doi.org/10.1093/mnras/stz740>
- Hirota T., Machida M. N., Matsushita Y., Motogi K., Matsumoto N., Kim M. K., Burns R. A., Honma M. (2017) Disk-driven rotating bipolar outflow in Orion Source I. *Nature Astronomy*, 1:0146. <https://doi.org/10.1038/s41550-017-0146>
- Jhan K.-S., Lee C.-F. (2016) A Multi-epoch SMA Study of the HH 211 Protostellar Jet: Jet Motion and Knot Formation. *ApJ*, 816:32. <https://doi.org/10.3847/0004-637X/816/1/32>
- Jiménez-Serra I., Martín-Pintado J., Rodríguez-Franco A., Martín S. (2005) Grain Evolution across the Shocks in the L1448-mm Outflow. *ApJ*, 627:L121-L124. <https://doi.org/10.1086/432467>
- Kennicutt R. C., Evans N. J. (2012) Star Formation in the Milky Way and Nearby Galaxies. *ARA&A*, 50:531-608. <https://doi.org/10.1146/annurev-astro-081811-125610>
- Königl A., Pudritz R. E. (2000) Disk Winds and the Accretion-Outflow Connection. *Protostars and Planets IV*, 759. <https://doi.org/>
- Kwon W., Fernández-López M., Stephens I. W., Looney L. W. (2015) Kinematics of the Envelope and Two Bipolar Jets in the Class 0 Protostellar System L1157. *ApJ*, 814:43. <https://doi.org/10.1088/0004-637X/814/1/43>

- Larson R. B. (1969) Numerical calculations of the dynamics of collapsing proto-star. *MNRAS*, 145:271. <https://doi.org/10.1093/mnras/145.3.271>
- Launhardt R., Pavlyuchenkov Y., Gueth F., Chen X., Dutrey A., Guilloteau S., Henning T., Piétu V., Schreyer K., Semenov D. (2009) Rotating molecular outflows: the young T Tauri star in CB 26. *A&A*, 494:147-156. <https://doi.org/10.1051/0004-6361:200810835>
- Lee C.-F., Mundy L. G., Reipurth B., Ostriker E. C., Stone J. M. (2000) CO Outflows from Young Stars: Confronting the Jet and Wind Models. *ApJ*, 542:925-945. <https://doi.org/10.1086/317056>
- Lee C.-F., Stone J. M., Ostriker E. C., Mundy L. G. (2001) Hydrodynamic Simulations of Jet- and Wind-driven Protostellar Outflows. *ApJ*, 557:429-442. <https://doi.org/10.1086/321648>
- Lee C.-F., Ho P. T. P. (2005) Outflow Interaction in the Late Stages of Star Formation. *ApJ*, 624:841-852. <https://doi.org/10.1086/429535>
- Lee C.-F., Ho P. T. P., Hirano N., Beuther H., Bourke T. L., Shang H., Zhang Q. (2007) HH 212: Submillimeter Array Observations of a Remarkable Protostellar Jet. *ApJ*, 659:499-511. <https://doi.org/10.1086/512540>
- Lee C.-F., Ho P. T. P., Bourke T. L., Hirano N., Shang H., Zhang Q. (2008) SiO Shocks of the Protostellar Jet HH 212: A Search for Jet Rotation. *ApJ*, 685:1026-1032. <https://doi.org/10.1086/591177>
- Lee C.-F., Hirano N., Palau A., Ho P. T. P., Bourke T. L., Zhang Q., Shang H. (2009) Rotation and Outflow Motions in the Very Low-Mass Class 0 Protostellar System HH 211 at Subarcsecond Resolution. *ApJ*, 699:1584-1594. <https://doi.org/10.1088/0004-637X/699/2/1584>
- Lee C.-F., Hasegawa T. I., Hirano N., Palau A., Shang H., Ho P. T. P., Zhang Q. (2010) The Reflection-Symmetric Wiggle of the Young Protostellar Jet HH 211. *ApJ*, 713:731-737. <https://doi.org/10.1088/0004-637X/713/2/731>
- Lee C.-F. (2010) A Change of Rotation Profile in the Envelope in the HH 111 Protostellar System: A Transition to a Disk?. *ApJ*, 725:712-720. <https://doi.org/10.1088/0004-637X/725/1/712>
- Lee C.-F., Hirano N., Zhang Q., Shang H., Ho P. T. P., Mizuno Y. (2015) Jet Motion, Internal Working Surfaces, and Nested Shells in the Protostellar System HH 212. *ApJ*, 805:186. <https://doi.org/10.1088/0004-637X/805/2/186>
- Lee C.-F., Hwang H.-C., Li Z.-Y. (2016) Angular Momentum Loss in the Envelope-Disk Transition Region of the HH 111 Protostellar System: Evidence for Magnetic Braking?. *ApJ*, 826:213. <https://doi.org/10.3847/0004-637X/826/2/213>
- Lee C.-F., Li Z.-Y., Ho P. T. P., Hirano N., Zhang Q., Shang H. (2017a) First detection of equatorial dark dust lane in a protostellar disk at submillimeter wavelength. *Science Advances*, 3:e1602935. <https://doi.org/10.1126/sciadv.1602935>
- Lee C.-F., Li Z.-Y., Ho P. T. P., Hirano N., Zhang Q., Shang H. (2017b) Formation and Atmosphere of Complex Organic Molecules of the HH 212 Protostellar Disk. *ApJ*, 843:27. <https://doi.org/10.3847/1538-4357/aa7757>
- Lee C.-F., Ho P. T. P., Li Z.-Y., Hirano N., Zhang Q., Shang H. (2017c) A rotating protostellar jet launched from the innermost disk of HH 212. *Nature Astronomy*, 1:0152. <https://doi.org/10.1038/s41550-017-0152>
- Lee C.-F., Li Z.-Y., Codella C., Ho P. T. P., Podio L., Hirano N., Shang H., Turner N. J., Zhang Q. (2018a) A 100 au Wide Bipolar Rotating Shell Emanating from the HH 212 Protostellar Disk: A Disk Wind?. *ApJ*, 856:14. <https://doi.org/10.3847/1538-4357/aaae6d>
- Lee C.-F., Li Z.-Y., Hirano N., Shang H., Ho P. T. P., Zhang Q. (2018b) ALMA Observations of the Very Young Class 0 Protostellar System HH211-mms: A 30 au Dusty Disk with a Disk Wind Traced by SO?. *ApJ*, 863:94. <https://doi.org/10.3847/1538-4357/aad2da>
- Lee C.-F., Hwang H.-C., Ching T.-C., Hirano N., Lai S.-P., Rao R., Ho P. T. P. (2018c) Unveiling a magnetized jet from a low-mass protostar. *Nature Communications*, 9:4636. <https://doi.org/10.1038/s41467-018-07143-8>
- Lee C.-F., Kwon W., Jhan K.-S., Hirano N., Hwang H.-C., Lai S.-P., Ching T.-C., Rao R., Ho P. T. P. (2019a) A Pseudodisk Threaded with a Toroidal and Pinched Poloidal Magnetic Field Morphology in the HH 211 Protostellar System. *ApJ*, 879:101. <https://doi.org/10.3847/1538-4357/ab2458>

- Lee C.-F., Li Z.-Y., Turner N. J. (2019b) Spiral structures in an embedded protostellar disk driven by envelope accretion. *Nature Astronomy*, 466. <https://doi.org/10.1038/s41550-019-0905-x>
- Louvet F., Dougados C., Cabrit S., Mardones D., Ménard F., Tabone B., Pinte C., Dent W. R. F. (2018) The HH30 edge-on T Tauri star. A rotating and precessing monopolar outflow scrutinized by ALMA. *A&A*, 618:A120. <https://doi.org/10.1051/0004-6361/201731733>
- Machida M. N., Inutsuka S.-. ichiro ., Matsumoto T. (2008) High- and Low-Velocity Magnetized Outflows in the Star Formation Process in a Gravitationally Collapsing Cloud. *ApJ*, 676:1088-1108. <https://doi.org/10.1086/528364>
- Marti J., Rodriguez L. F., Reipurth B. (1993) HH 80-81: A Highly Collimated Herbig-Haro Complex Powered by a Massive Young Star. *ApJ*, 416:208. <https://doi.org/10.1086/173227>
- Masciadri E., Raga A. C. (2002) Herbig-Haro Jets from Orbiting Sources. *ApJ*, 568:733-742. <https://doi.org/10.1086/338767>
- Masunaga H., Inutsuka S.-. ichiro . (2000) A Radiation Hydrodynamic Model for Protostellar Collapse. II. The Second Collapse and the Birth of a Protostar. *ApJ*, 531:350-365. <https://doi.org/10.1086/308439>
- Maury A. J., André P., Testi L., et al. (2019) Characterizing young protostellar disks with the CALYPSO IRAM-PdBI survey: large Class 0 disks are rare. *A&A*, 621:A76. <https://doi.org/10.1051/0004-6361/201833537>
- McCaughrean M. J., Rayner J. T., Zinnecker H. (1994) Discovery of a Molecular Hydrogen Jet near IC 348. *ApJ*, 436:L189. <https://doi.org/10.1086/187664>
- McCaughrean M., Zinnecker H., Andersen M., Meeus G., Lodieu N. (2002) Standing on the shoulder of a giant: ISAAC, Antu, and star formation. *The Messenger*, 109:28-36. <https://doi.org/>
- McKee C. F., Ostriker E. C. (2007) Theory of Star Formation. *ARA&A*, 45:565-687. <https://doi.org/10.1146/annurev.astro.45.051806.110602>
- Millan-Gabet R., Malbet F., Akeson R., Leinert C., Monnier J., Waters R. (2007) The Circumstellar Environments of Young Stars at AU Scales. *Protostars and Planets V.*, 539. <https://doi.org/>
- Mizuno Y., Hardee P. E., Nishikawa K.-I. (2014) Spatial Growth of the Current-driven Instability in Relativistic Jets. *ApJ*, 784:167. <https://doi.org/10.1088/0004-637X/784/2/167>
- Moraghan A., Lee C.-F., Huang P.-S., Vaidya B. (2016) A study of the wiggle morphology of HH 211 through numerical simulations. *MNRAS*, 460:1829-1838. <https://doi.org/10.1093/mnras/stw1089>
- Noriega-Crespo A., Raga A. C., Lora V., Stapelfeldt K. R., Carey S. J. (2011) The Precession of the Herbig-Haro 111 Flow in the Infrared. *ApJ*, 732:L16. <https://doi.org/10.1088/2041-8205/732/1/L16>
- Ostriker E. C., Lee C.-F., Stone J. M., Mundy L. G. (2001) A Ballistic Bow Shock Model for Jet-driven Protostellar Outflow Shells. *ApJ*, 557:443-450. <https://doi.org/10.1086/321649>
- Ouyed R., Clarke D. A., Pudritz R. E. (2003) Three-dimensional Simulations of Jets from Keplerian Disks: Self-regulatory Stability. *ApJ*, 582:292-319. <https://doi.org/10.1086/344507>
- Palau A., Ho P. T. P., Zhang Q., Estalella R., Hirano N., Shang H., Lee C.-F., Bourke T. L., Beuther H., Kuan Y.-J. (2006) Submillimeter Emission from the Hot Molecular Jet HH 211. *ApJ*, 636:L137-L140. <https://doi.org/10.1086/500242>
- Pérez L. M., Carpenter J. M., Andrews S. M., et al. (2016) Spiral density waves in a young protoplanetary disk. *Science*, 353:1519-1521. <https://doi.org/10.1126/science.aaf8296>
- Plunkett A. L., Arce H. G., Mardones D., van Dokkum P., Dunham M. M., Fernández-López M., Gallardo J., Corder S. A. (2015) Episodic molecular outflow in the very young protostellar cluster Serpens South. *Nature*, 527:70-73. <https://doi.org/10.1038/nature15702>
- Podio L., Codella C., Gueth F., et al. (2015) The jet and the disk of the HH 212 low-mass protostar imaged by ALMA: SO and SO<sub>2</sub> emission. *A&A*, 581:A85. <https://doi.org/10.1051/0004-6361/201525778>
- Podio L., Codella C., Gueth F., et al. (2016) First image of the L1157 molecular jet by the CALYPSO IRAM-PdBI survey. *A&A*, 593:L4. <https://doi.org/10.1051/0004->

- 6361/201628876
- Podio L. (2017) Protostellar Jets: The Revolution with ALMA. Workshop sull'Astronomia Millimetrica in Italia,:23. <https://doi.org/10.5281/zenodo.1117656>
- Pudritz R. E., Ouyed R., Fendt C., Brandenburg A. (2007) Disk Winds, Jets, and Outflows: Theoretical and Computational Foundations. *Protostars and Planets V*,:277. <https://doi.org/>
- Pudritz R. E., Hardcastle M. J., Gabuzda D. C. (2012) Magnetic Fields in Astrophysical Jets: From Launch to Termination. *Space Sci. Rev.*, 169:27-72. <https://doi.org/10.1007/s11214-012-9895-z>
- Pudritz R. E., Ray T. P. (2019) The Role of Magnetic Fields in Protostellar Outflows and Star Formation. *Frontiers in Astronomy and Space Sciences*, 6:54. <https://doi.org/10.3389/fspas.2019.00054>
- Raga A. C., Canto J., Binette L., Calvet N. (1990) Stellar Jets with Intrinsically Variable Sources. *ApJ*, 364:601. <https://doi.org/10.1086/169443>
- Raga A. C., Canto J., Biro S. (1993) Ballistic stellar jets from sources with a time-dependent ejection direction. *MNRAS*, 260:163-170. <https://doi.org/10.1093/mnras/260.1.163>
- Raga A. C., Velázquez P. F., Cantó J., Masciadri E. (2002) The time-dependent ejection velocity histories of HH 34 and HH 111. *A&A*, 395:647-656. <https://doi.org/10.1051/0004-6361:20021180>
- Raga A. C., Esquivel A., Velázquez P. F., Cantó J., Haro-Corzo S., Riera A., Rodríguez-González A. (2009) Mirror and Point Symmetries in a Ballistic Jet from a Binary System. *ApJ*, 707:L6-L11. <https://doi.org/10.1088/0004-637X/707/1/L6>
- Ray T., Dougados C., Bacciotti F., Eisloffel J., Chrysostomou A. (2007) Toward Resolving the Outflow Engine: An Observational Perspective. *Protostars and Planets V*,:231. <https://doi.org/>
- Reipurth B. (2000) Disintegrating Multiple Systems in Early Stellar Evolution. *AJ*, 120:3177-3191. <https://doi.org/10.1086/316865>
- Reipurth B., Bally J. (2001) Herbig-Haro Flows: Probes of Early Stellar Evolution. *ARA&A*, 39:403-455. <https://doi.org/10.1146/annurev.astro.39.1.403>
- Reipurth B., Rodríguez L. F., Anglada G., Bally J. (2002) Radio Continuum Maps of Deeply Embedded Protostars: Thermal Jets, Multiplicity, and Variability. *AJ*, 124:1045-1053. <https://doi.org/10.1086/341172>
- Reipurth B., Rodríguez L. F., Anglada G., Bally J. (2004) Radio Continuum Jets from Protostellar Objects. *AJ*, 127:1736-1746. <https://doi.org/10.1086/381062>
- Reipurth B., Davis C. J., Bally J., Raga A. C., Bowler B. P., Geballe T. R., Aspin C., Chiang H.-F. (2019) The Giant Herbig-Haro Flow HH 212 and Associated Star Formation. *AJ*, 158:107. <https://doi.org/10.3847/1538-3881/ab2d25>
- Reiter M., Kiminki M. M., Smith N., Bally J. (2017) Proper motions of collimated jets from intermediate-mass protostars in the Carina Nebula. *MNRAS*, 470:4671-4697. <https://doi.org/10.1093/mnras/stx1489>
- Riaz B., Briceño C., Whelan E. T., Heathcote S. (2017) First Large-scale Herbig-Haro Jet Driven by a Proto-brown Dwarf. *ApJ*, 844:47. <https://doi.org/10.3847/1538-4357/aa70e8>
- Rodríguez L. F. (1997) Thermal Radio Jets. *Herbig-Haro Flows and the Birth of Stars*, 182:83-92. <https://doi.org/>
- Rodríguez L. F., Zapata L. A., Palau A. (2014) JVLA Observations of IC 348 SW: Compact Radio Sources and their Nature. *ApJ*, 790:80. <https://doi.org/10.1088/0004-637X/790/1/80>
- Rodríguez-Kamenetzky A., Carrasco-González C., Araudo A., Romero G. E., Torrelles J. M., Rodríguez L. F., Anglada G., Martí J., Perucho M., Valotto C. (2017) The Highly Collimated Radio Jet of HH 80-81: Structure and Nonthermal Emission. *ApJ*, 851:16. <https://doi.org/10.3847/1538-4357/aa9895>
- Santiago-García J., Tafalla M., Johnstone D., Bachiller R. (2009) Shells, jets, and internal working surfaces in the molecular outflow from IRAS 04166+2706. *A&A*, 495:169-181. <https://doi.org/10.1051/0004-6361:200810739>
- Schilke P., Walmsley C. M., Pineau des Forets G., Flower D. R. (1997) SiO production in interstellar shocks. *A&A*, 321:293-304. <https://doi.org/>

- Shang H., Allen A., Li Z.-Y., Liu C.-F., Chou M.-Y., Anderson J. (2006) A Unified Model for Bipolar Outflows from Young Stars. *ApJ*, 649:845-855. <https://doi.org/10.1086/506513>
- Shu F. H., Najita J., Ostriker E. C., Shang H. (1995) Magnetocentrifugally Driven Flows from Young Stars and Disks. V. Asymptotic Collimation into Jets. *ApJ*, 455:L155. <https://doi.org/10.1086/309838>
- Shu F. H., Najita J. R., Shang H., Li Z.-Y. (2000) X-Winds Theory and Observations. *Protostars and Planets IV*, 789-814. <https://doi.org/>
- Simon M., Dutrey A., Guilloteau S. (2000) Dynamical Masses of T Tauri Stars and Calibration of Pre-Main-Sequence Evolution. *ApJ*, 545:1034-1043. <https://doi.org/10.1086/317838>
- Stahler S. W. (1988) Deuterium and the Stellar Birthline. *ApJ*, 332:804. <https://doi.org/10.1086/166694>
- Stone J. M., Norman M. L. (1993) Numerical Simulations of Protostellar Jets with Nonequilibrium Cooling. II. Models of Pulsed Jets. *ApJ*, 413:210. <https://doi.org/10.1086/172989>
- Suttner G., Smith M. D., Yorke H. W., Zinnecker H. (1997) Multi-dimensional numerical simulations of molecular jets.. *A&A*, 318:595-607. <https://doi.org/>
- Tabone B., Cabrit S., Bianchi E., Ferreira J., Pineau des Forêts G., Codella C., Gusdorf A., Gueth F., Podio L., Chapillon E. (2017) ALMA discovery of a rotating SO/SO<sub>2</sub> flow in HH212. A possible MHD disk wind?. *A&A*, 607:L6. <https://doi.org/10.1051/0004-6361/201731691>
- Tafalla M., Su Y.-N., Shang H., Johnstone D., Zhang Q., Santiago-García J., Lee C.-F., Hirano N., Wang L.-Y. (2017) Anatomy of the internal bow shocks in the IRAS 04166+2706 protostellar jet. *A&A*, 597:A119. <https://doi.org/10.1051/0004-6361/201629493>
- Takahashi S., Machida M. N., Tomisaka K., Ho P. T. P., Fomalont E. B., Nakanishi K., Girart J. M. (2019) ALMA High Angular Resolution Polarization Study: An Extremely Young Class 0 Source, OMC-3/MMS 6. *ApJ*, 872:70. <https://doi.org/10.3847/1538-4357/aaf6ed>
- Takami M., Karr J. L., Nisini B., Ray T. P. (2011) A Detailed Study of Spitzer-IRAC Emission in Herbig-Haro Objects. II. Interaction between Ejecta and Ambient Gas. *ApJ*, 743:193. <https://doi.org/10.1088/0004-637X/743/2/193>
- Takami M., Fu G., Liu H. B., et al. (2018) Near-infrared High-resolution Imaging Polarimetry of FU Ori-type Objects: Toward a Unified Scheme for Low-mass Protostellar Evolution. *ApJ*, 864:20. <https://doi.org/10.3847/1538-4357/aad2e1>
- Terquem C., Eislöffel J., Papaloizou J. C. B., Nelson R. P. (1999) Precession of Collimated Outflows from Young Stellar Objects. *ApJ*, 512:L131-L134. <https://doi.org/10.1086/311880>
- Tobin J. J., Looney L. W., Li Z.-Y., et al. (2016) The VLA Nascent Disk and Multiplicity Survey of Perseus Protostars (VANDAM). II. Multiplicity of Protostars in the Perseus Molecular Cloud. *ApJ*, 818:73. <https://doi.org/10.3847/0004-637X/818/1/73>
- Tomida K., Machida M. N., Hosokawa T., Sakurai Y., Lin C. H. (2017) Grand-design Spiral Arms in a Young Forming Circumstellar Disk. *ApJ*, 835:L11. <https://doi.org/10.3847/2041-8213/835/1/L11>
- Vorobyov E. I., Basu S. (2005) The Origin of Episodic Accretion Bursts in the Early Stages of Star Formation. *ApJ*, 633:L137-L140. <https://doi.org/10.1086/498303>
- Whelan E. T., Ray T. P., Bacciotti F., Natta A., Testi L., Randich S. (2005) A resolved outflow of matter from a brown dwarf. *Nature*, 435:652-654. <https://doi.org/10.1038/nature03598>
- Wilner D. J., Reid M. J., Menten K. M. (1999) The Synchrotron Jet from the H<sub>2</sub>O Maser Source in W3(OH). *ApJ*, 513:775-779. <https://doi.org/10.1086/306907>
- Woitaj J., Ray T. P., Bacciotti F., Davis C. J., Eislöffel J. (2002) Hubble Space Telescope Space Telescope Imaging Spectrograph Observations of the Bipolar Jet from RW Aurigae: Tracing Outflow Asymmetries Close to the Source. *ApJ*, 580:336-342. <https://doi.org/10.1086/343124>
- Yen H.-W., Takakuwa S., Ohashi N. (2010) High-Velocity Jets and Slowly Rotating Envelope in B335. *ApJ*, 710:1786-1799. <https://doi.org/10.1088/0004-637X/710/2/1786>
- Yen H.-W., Koch P. M., Takakuwa S., Krasnopolsky R., Ohashi N., Aso Y. (2017) Signs of Early-stage Disk Growth Revealed with ALMA. *ApJ*, 834:178.

- <https://doi.org/10.3847/1538-4357/834/2/178>
- Zapata L. A., Ho P. T. P., Rodríguez L. F., O'Dell C. R., Zhang Q., Muench A. (2006) Silicon Monoxide Observations Reveal a Cluster of Hidden Compact Outflows in the OMC 1 South Region. *ApJ*, 653:398-408. <https://doi.org/10.1086/508319>
- Zapata L. A., Schmid-Burgk J., Muders D., Schilke P., Menten K., Guesten R. (2010) A rotating molecular jet in Orion. *A&A*, 510:A2. <https://doi.org/10.1051/0004-6361/200810245>
- Zinnecker H., McCaughrean M. J., Rayner J. T. (1998) A symmetrically pulsed jet of gas from an invisible protostar in Orion. *Nature*, 394:862-865. <https://doi.org/10.1038/29716>